ISSN 0915-633X

NATIONAL INSTITUTE FOR FUSION SCIENCE

Design-Relevant Mechanical Properties of 316-Type Stainless Steels for Superconducting Magnets

R.L. Tobler, A. Nishimura and J. Yamamoto

(Received - July 5, 1996)

NIFS-430 Aug. 1996

RESEARCH REPORT
NIFS Series

NAGOYA, JAPAN

DESIGN-RELEVANT MECHANICAL PROPERTIES OF 316-TYPE STAINLESS STEELS FOR SUPERCONDUCTING MAGNETS

R.L. Tobler*, A. Nishimura, and J. Yamamoto
National Institute for Fusion Science
Toki, Gifu, Japan

Abstract

Worldwide interest in austenitic alloys for structural applications in superconducting magnets has led to an expanded database for the 316-type stainless steels. We review the cryogenic mechanical properties of wrought, cast, and welded steels at liquid helium temperature (4 K), focussing on aspects of material behavior relevant to magnet design. Fracture mechanics parameters essential to structural reliability assessments are presented, including strength, toughness, and fatigue parameters that are critical for some component designs.

Contents

* Visiting researcher from National Institute of Standards and Technology, Boulder, Co, USA.

1. Introduction

Superconducting magnets generating high magnetic fields are used to contain plasma in experimental fusion machines and prototype reactors. The magnet windings are superconducting NbTi or Nb_3Sn strands that are bundled and jacketed in conduits and cooled with supercritical helium near 4.5 K. Inevitably the conduit sheaths and other magnet support structures are austenitic stainless steels or superalloys that are highly stressed in environments more demanding than those in traditional cryogenic applications.

Steels for primary members may constitute half the total weight of magnet structures. Many factors are considered in materials selection to minimize weight, conserve space, and sustain the large magnetic forces safely. Selection is based largely on mechanical properties, fabricability, and cost. Mechanical failure is unacceptable in view of cost and safety issues. Fracture mechanics is used to reduce the probability of failure, and nuclear-class safety regulations apply to structural integrity assessments for prototye fusion devices.

The 304-type steels used in early designs are being supplanted by 316-type steels in recent applications. SUS 316 is the primary alloy used in the Large Helical Device (LHD) now under construction in Japan [1], while 316LN leads the candidates for next-generation tokamaks such as the International Thermonuclear Experimental Reactor (ITER) [2]. The 316-type steels offer greater microstructural and magnetic stability compared to the 304-type predecessors, and 316LN offers higher strength at the same toughness level compared to its counterpart, 304LN.

The potential failure modes of basic structural components and the performance limits of some candidate materials have been identified recently [3-6]. Other papers describe stainless steels in general and discuss improvements needed in their databases [7-9]. For 316-type steels, we provide here a collection of references with an overview of relevant data and mechanical behavior at 4 K. The references are loosely organized by topics: physical properties [10-20], uniaxial tensile properties including yield strength, yield-point anomalies, and creep [21-48], fracture toughness [49-70], properties of castings and welds [71-93], and fatigue [94-105].

2. Steel Forms and Compositions

2.1 Wrought Products

The base composition of AISI 316 is Fe, 16-18[Cr], 10-14[Ni], 2-3[Mo]. At 295 K this steel is nonmagnetic. It is a relatively low yield strength steel with high work-hardening capability, ductility, and toughness. The steel may be hardened and strengthened by cold-work, but the annealed condition is specified for magnet applications since they require relatively thick sections

Table 1. Selected Physical Properties of 316 Steel [7].

Property		Temperature, K		
		295	77	4
Young's Modulus	GPa	195	209	208
Shear Modulus	GPa	75.2	81.6	81.0
Poisson Ratio	-	0.294	0.283	0.282
Electrical Resistivity	$m\Omega \cdot cm$	75.0	56.6	53.9
Thermal Expansion	$K^{-1} \cdot 10^{-6}$	15.8	13.0	10.2
Thermal Conductivity	$W \cdot m^{-1} \cdot K^{-1}$	14.7	7.9	0.28
Specific Heat	$J \cdot kg^{-1} \cdot K^{-1}$	480	19	1.9

Table 2. Specified Chemical Compositions for 316-type Stainless Steels in Various Forms.

	C	N	Cr	Ni	Mo	Mn	Si
Wrought Forms:							
SUS 316L	0.03 max		16.00-18.00	12.00-15.00	2.00-3.00	2.00 max	1.00 max
SUS 316	0.08 max		16.00-18.00	10.00-14.00	2.00-3.00	2.00 max	1.00 max
SUS 316LN	0.03 max	0.12-0.22	16.00-18.50	10.50-14.50	2.00-3.00	2.00 max	1.00 max
SUS 316N	0.08 max	0.10-0.22	16.00-18.00	10.00-14.00	2.00-3.00	2.00 max	1.00 max
AISI 316L	0.03 max	0.02-0.05	16.00-18.00	10.00-14.00	2.00-3.00	2.00 max	1.00 max
AISI 316	0.08 max	0.02-0.05	"	"			
AISI 316LN	0.03 max	0.18-0.25	"	"			
AISI 316N	0.08 max	0.18-0.25	"	"			
Castings:							
CF-3M	0.03 max		17.00-21.00	9.00-13.00	2.00-3.00	1.50 max	1.50 max
CF-8M	0.08 max		18.00-21.00	9.00-12.00	2.00-3.00	1.50 max	1.50 max
Weld Electrodes (Covered):							
E316	0.08 max		17.00-20.00	11.00-14.00	1.00-2.00	2.50 max	0.90 max
E316L	0.04 max		17.00-20.00	11.00-14.00			
Weld Electrode (Rod or Bare):							
ER316	0.03, max		18.00-20.00	11.00-14.00	2.00-3.00	1.00-2.50	0.25-0.60

and welding. Table 1 lists useful physical properties assembled from handbooks [7].

The principal grades of wrought steels in the 316 family are listed in Table 2. Included are 316L (low C), 316LN (low C, high N), and 316N (high N). Low-carbon "L" grades (0.03C, max) are preferred to normal-grades (0.08C, max) in applications requiring welding. In addition, certain manufacturers on limited scales have produced microalloyed versions of the LN grade to resist sensitization as discussed later in the text.

The microstructures of wrought steels are normally 100% austenite (γ). Iron's equilibrium structure at room temperature and below is body-centered cubic, but austenite with the face-centered-cubic atomic arrangement is achieved by alloy additions of Cr, Ni, Mn, and other elements. The austenite is metastable: it resists transformation on cooling to 4 K but transforms when deformed at cryogenic temperatures [10, 11].

2.2 Castings

Castings offer economic advantages over wrought products in special applications where extraordinary size or complex shapes are required. Previous cryogenic uses of austenitic steel castings include bubble chamber bodies and magnet tubes. Most castings have a multiphase structure with lower cryogenic toughness compared to wrought steel; nevertheless, it is possible to produce single-phase austenitic castings having 4-K strength and toughness combinations nearly equivalent to the wrought products.

In terms of the Alloy Castings Institute designations, CF-3M and CF-8M are the cast counterparts of AISI 316L and AISI 316, respectively. The corresponding cast and wrought product compositions are not identical. A cast microstructure is typically a mixture of delta ferrite δ within the γ matrix. Ferrite in castings and welds alike is a major factor influencing the cryogenic mechanical properties. Depending on the details of manufacturing and composition, from 0 to 40% ferrite is possible in the castings. The amount is predictable from Schoefer's constitution diagram [12].

2.3 Weld Fillers

Traditional 308L and 316L fillers are commonly used to join the 316-type steels for cryogenic service. The fillers have broad composition ranges, and their properties can be varied by compositional shifts within the allowable ranges. The microstructure of a deposit is fixed mainly by the choice of the filler composition, and the amounts of microstructural constituents can be predicted using the constitution diagrams developed by Schaeffler [13] and DeLong [14]. The as-deposited microstructures of 316L fillers typically contain some ferrite to prevent hot cracking during welding. The targetted structure is usually austenite plus ferrite, with at least 3% ferrite. Otherwise, modified or unrestricted compositions may be selected to completely eliminate ferrite and produce a more fracture-resistant single-phase austenitic structure.

3. Martensitic Transformations

The 316-type steels, although austenitic at room temperature, will transform martensitically on straining at cryogenic temperatures. A martensitic transformation is a sudden shearing of atom groups that alters the crystal structure locally with no atomic diffusion. The fcc austenite (γ) partially transforms to bcc alpha (α') and hcp epsilon (ε) martensite phases:

$$\gamma \rightarrow \alpha' + \varepsilon \qquad (1)$$

The newly formed α' is ferromagnetic and readily detectable by magnetometry or other means (microscopy, heat-tinting, and magnetic filings). The nonferromagnetic epsilon may be detected using X-rays. Transformation kinetics depend on composition, temperature, stress or strain, and applied magnetic field. Data on field effects are just beginning to emerge and are considered later. Properties in zero magnetic field are considered here.

Transformation occurs when the temperature is low enough and the strain is high enough. For AISI 316 in tension (zero magnetic field), α' begins to form at temperatures below 175 K when a critical strain of about 2% is exceeded. The amount of transformation per unit strain increases as the temperature is lowered to 4 K [23]. In liquid helium, straining to fracture may produce more than 80% α' while the amount of ε peaks near 20% at intermediate strains and then decreases near fracture. Increasing the C or N will modify the transformation characteristics by increasing the critical strain slightly and decreasing the amount of transformation product per unit strain.

The following property changes are associated with martensitic transformations in these steels should be anticipated in design:

3.1 Magnetic Properties

As stated earlier, bcc martensite is ferromagnetic, whereas the original austenite and hcp martensite phases are not. So in magnet systems where ferromagnetism is not tolerable, it is necessary to select a sufficiently stable steel composition. Suzuki et al proposed a modified fatigue failure criterion to take this factor explicitly into account [95].

3.2 Volumetric Expansion

A volume expansion not exceeding 3% accompanies the martensitic transformation. Potential consequences of expansion include loss of tolerances in critically machined parts, loosening of bolts, and the creation of residual stresses. Potential loss of dimensional tolerances affected steel selection for the Isabelle magnet tubes [71]. Localized residual stress created by transformation in crack-tip plastic zones is a factor affecting the growth rates of fatigue cracks at 4 K [8].

3.3 Mechanical Properties

Although martensitic transformations are capable of influencing any mechanical properties, the effects in 316-type steels are not necessarily of great concern. The austenite stability of these steels is relatively high, and normally transformation is not expected unless the yield stress YS is exceeded. Noteworthy effects are cited in the text where appropriate.

4. Magnetic Properties

Wrought and annealed 316-type steels with the austenitic microstructure are superparamagnetic. Magnetic permeability values are commonly quoted for as-received steels in the initial condition at room temperature. During low temperature service the permeability value may be altered by reversible changes at the Neel transition, or by irreversible changes accompanying martensitic phase transformations.

4.1 Reversible Change

Magnetic susceptibility measurements for the 316-type steels show a cusp-like maximum at cryogenic temperatures, the height and sharpness of which depends on the magnitude of the applied

magnetic field. Apparently, a small volume of the material exists as noninteracting ferromagnetic clusters embedded in a matrix that undergoes a spin-glass transition. At low temperatures these clusters interact with each other, and with the matrix. These interactions cause the magnetic susceptibility maximum to shift to lower temperatures and vanish at high fields [16-18].

The temperature at which the magnetic ordering or spin-glass transition takes place is the Neel temperature, T_N. For a given composition, T_N is predictable. It depends on the concentration of base alloying elements, but not on interstitials such as C and N. Based on the composition limits listed in Table 2, T_N for the AISI 316 steels lies in the range 1.5 to 43 K, and the mean specification corresponds to T_N = 22.5 K [15].

4.2 Irreversible Change

The 316-type steels are superparamagnetic if a fully austenitic structure prevails, but not if measurable amounts of δ or α' martensite are present. The δ and α' phases are both ferromagnetic. Typically, δ is found in castings and welds as a second phase dispersed in rapidly solidified austenite. The magnetic permeability of castings and welds is therefore relatively high (typically 1.01 to 1.60) compared to wrought steels (typically 1.001).

The stability of austenite increases with alloying, especially with C, N, and Ni additions. The temperatures M_S and M_d in zero magnetic field can be predicted [10, 11]. M_S is the martensite start temperature, below which some martensite forms spontaneously on cooling. M_d is the temperature below which martensite begins to form with deformation. The calculated transformation temperatures involve some uncertainties because the predictive equations were developed for compression, for a set of materials including many low-alloy steels, for specific strain or martensite levels, and with no accounting for trace elements.

The presence of δ or α' in any grade affects the cryogenic mechanical properties while introducing ferromagnetism. No α' martensite is found in properly homogenized wrought products, and none forms spontaneously on cooling to 4 K. However, α' forms in substantial quantities along with some ε when the steels are cryogenically deformed (see later text). Therefore, the magnetic permeability of cryogenic components increases if martensite is induced by monotonic or cyclic strains, or by thermal strains from cold thermal fatigue [3]. The resulting permeability increase is permanent and can have undesirable effects, such as undermining the homogeneity of magnetic fields or spawning electromagnetic forces due to eddy currents [95].

5. Elastic Properties

The elastic constants are known precisely from ultrasonic studies [18-20]. For AISI 316, measurements of Poisson's ratio and the various elastic moduli of engineering interest (Young's, longitudinal, shear, and bulk) have been usefully tabulated at selected temperatures between 300 and 0 K [19]. Results are reproduced in Table 1 and Fig. 1.

The elastic moduli are anomalous at cryogenic temperatures. When plotted as a function of temperature, they peak at the Neel temperature and then fall slightly instead of plateauing near absolute zero. The anomalies are not very great in engineering terms, less than 1%. But since they occur near T_N, between liquid nitrogen and helium temperatures, the elastic property values at 4 K are not higher than at 77 K.

Elastic properties are structure-insensitive, meaning they do not dependent strongly on factors such as cold work, heat treatment, or phase transformations. Base composition is the principal determining factor, and the effects of the principal alloying elements are known. Chromium increases the elastic stiffnesses, whereas Ni and Mn decrease them, and the interstitials C and N have negligable effects [20]. If these factors are taken into account, the data available for

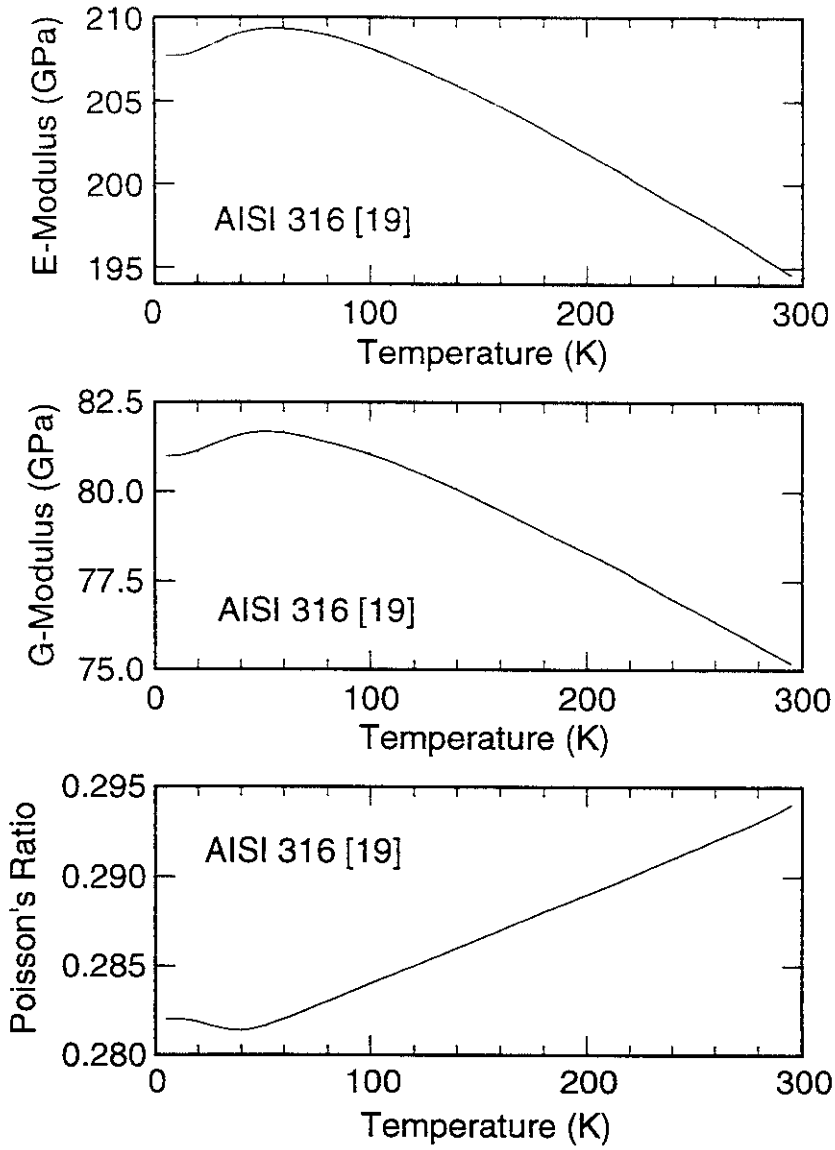

Figure 1. Elastic Constants for AISI 316 Stainless Steel.

AISI 316 should be useful for other grades in the 316-steel system.

Young's modulus is by definition the slope of the initial linear portion of the engineering stress-strain curve. A standard procedure for determining this parameter at liquid helium and other fixed-point temperatures exists in ASTM E 111-82. Mechanically measured Young's moduli are frequently reported along with other basic tensile properties at 295, 77, and 4 K. The precision of mechanical measurements (10%) is larger than that of ultrasonic measurements (2%) [20].

6. Uniaxial Tensile Properties

Selected tensile properties for wrought steels are shown in Fig. 2 and Table 3. These data come from standard tests, and they fairly represent the property ranges available for commercially annealed 316L, 316, and 316LN plates. Measurements are most commonly reported at three fixed-points: room, liquid nitrogen, and liquid helium temperature. Between 295 and 4 K, the amount of strengthening can be substantial while ductilty values remain high for all grades.

Strengthening at cryogenic temperatures is generally exponential, and the contribution of N in wrought steels, castings, and welds is outstanding. In Fig. 2, the essential difference between the

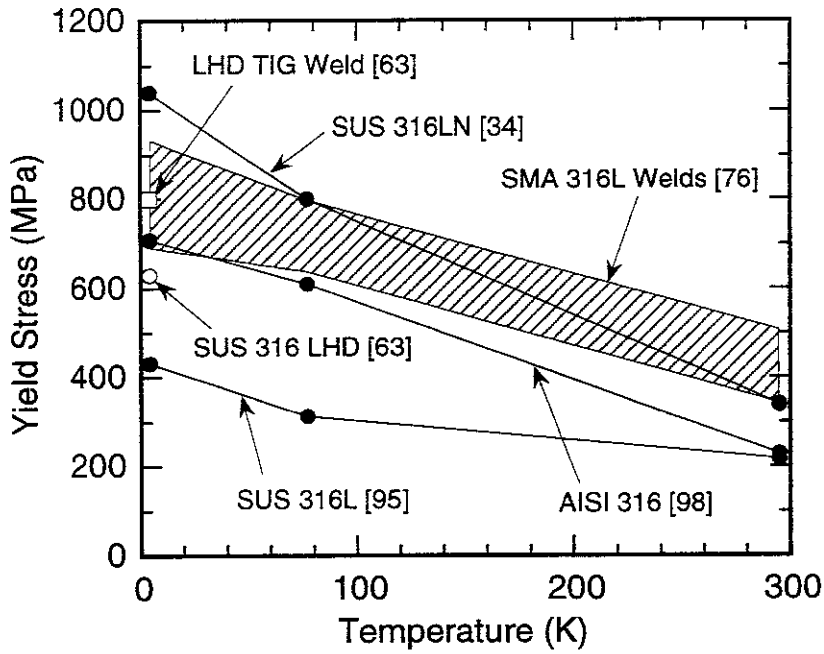

Figure 2. Tensile Yield Strengths of Selected Steels and Welds.

Table 3. Tensile Property Measurements for Three Wrought Steels.

Steel	[Ref.]	Temp (K)	YS (MPa)	UTS (MPa)	EL (%)	RA (%)
316L	[95]	300	216	530	65	73
		77	314	1235	49	61
		4	431	1440	48	62
316	[98]	295	228	575	56	73
		76	610	1240	62	70
		4	710	1300	48	57
316LN	[34]	293	340	715	72	85
		77	800	1520	75	70
		4	1040	1690	51	53

316L and 316LN grades is the N content (0.05 and 0.18%, respectively). As implied by the data in this figure, the difference in N content is mainly responsible for the YS spreads of nearly 125 MPa (at 295 K) and 610 MPa (at 4 K). The increment of strengthening at 4 K is much greater than that at 300 K. Large property spreads at cryogenic temperatures are evident in other mechanical properties as well.

6.1 Discontinuous Yielding

Tensile tests have been conducted at temperatures from 4 to 922 K [21-30]. The results demonstrate a unique material response near absolute zero that differs fundamentally from conventional behavior. Continuous, nearly isothermal deformation prevails at ambient temperature, but a stable-to-unstable deformation transition is encountered at approximately 30 K. Below this temperature, the tensile stress-strain curves at normal test speeds are serrated by discontinuous plastic flow events.

The distinctive features of discontinuous plastic flow at 4 K are audible acoustic emission, free-running plastic deformation, and localized specimen heating in the deforming zone. Deformation occurs in spurts at local regions within the gage length, owing to sudden "avalanches" of dislocation motion [30-32] Deformation velocities up to 26 mm/s have been measured during discontinuous elongation [43], and the specific heats and thermal conductivities are exceptionally low for steels near absolute zero (Table 1). Consequently, specimen temperature fluctuations cannot be avoided during tests in liquid helium. With each discontinuous yielding event, the temperature in local regions of the reduced section rises substantially above that of the surrounding helium cooling medium [32].

In standard cryogenic tension tests, the discontinuous yield stress DYS is defined as the value of the tensile stress at the first measurable instability event. For 316-type steels the DYS generally occurs at stresses and strains beyond the 0.2% offset YS. The DYS is temperature-sensitive and decreases with decreasing temperature below 30 K. At 4 K, the DYS also decreases if the specimen size or strain rate is increased, or if gaseous helium is substituted for liquid helium [32]. This sensitivity to material and test variables renders the DYS rather impractical for use as an engineering design parameter (see later Discussion).

6.2 Standard 4-K Tension Tests

Standard tension tests for metals in liquid helium have been developed recently in Japan and the United States. New standards were needed in view of the unique material behavior in this environment. According to the published procedures, JIS 2277 and ASTM E 1450-92, the test specimens are submerged in liquid helium and loaded in displacement control at strain rates less than 10^{-3}/s. The standard deviation of 4-K measurements has also been determined for a homogeneous material, to enable assessment of the variability of tensile property measurements made by these standards. Interlaboratory tests were conducted as part of the Versailles Advanced Materials And Standards (VAMAS) test program to provide this information [33-35]. Six laboratories performed 28 tensile tests for one heat of SUS 316LN steel in liquid helium. The results are shown in Table 4.

6.3 Metallurgical Determinants of Yield Stress

The YS at cryogenic temperatures is principally determined by two metallurgical factors: grain size and chemical composition. Data for AISI 316 and versions of SUS 316LN confirm that the YS is proportional to the inverse square root of the average grain diameter, D. For AISI 316 [23]:

$$YS = 180 + 190(D)^{-1/2} \text{ at 295 K, and} \qquad (2)$$

$$YS = 363 + 1505(D)^{-1/2} \text{ at 4 K.} \qquad (3)$$

The units are MPa for YS and μm for D. According to Eqs. (2) and (3), refining D from 155 to 20 μm raises the 295-K YS by only 27 MPa, while the 4-K YS is raised by 220 MPa. The result at 4 K is ten times the room temperature effect. Similar data are reported for the 316LN steels [36]. Thus, grain size effects, though negligable at 295 K, are potent at 4 K.

Table 4. Interlaboratory Tensile Test Results for SUS 316LN at 4 K [34].

	YS (MPa)	UTS (MPa)	EL (%)	RA (%)
Average Value	1065	1714	48.3	48.8
Standard Dev.	15	28	1.9	6.2

The effects of composition are likewise well documented. C and N strengthen appreciably without degrading ductility at cryogenic temperatures [37]. In practice C additions are limited since they produce precipitates at grain boundaries during hot-rolling operations [36-38]. The main strengthener is therefore N. Substitutional elements such as Mo, Cu, and V may provide secondary strengthening.

Two empirical equations were devised to express the 4-K YS of 316LN-grade steels based on the grain size and chemical contributions. The original expression developed by steel manufacturers is:

$$YS = 150 + 1700[C] + 2870[N] + 80[Mo] + 50(D)^{-1/2}, \quad (4)$$

where the YS at 4 K is in MPa, D is in mm, and the brackets indicate the composition of elements in mass % [36]. The second expression is:

$$YS = 316 + 2370[N] + 53.8[Mo] + 790(D)^{-1/2}, \quad (5)$$

where this time D is given in μm [39, 40]. Equation (5) has no [C] term; instead, the effect of C at levels below 0.03% is implicit in the constant which happens to be 316.

6.4 Temperature Dependence of Yield Stress

The existence of magnetic and elastic anomalies near T_N implies that the dislocation processes and mechanical behavior of these steels may be affected. Thus, possible links between the magnetic, elastic, and mechanical properties have been discussed for the 316-type steels and related Fe-Cr-Ni alloys at subzero temperatures. Three types of anomalous strength decreases have been reported in the Fe-Cr-Ni alloy system [26-28], but the effects were not always subsequently confirmed [22, 23, 29]. The anomalies are attributed to different physical processes that come into play at specific temperature intervals. They are: dislocation tunneling between 20 and 4 K, magnetic ordering at T_N between 60 and 35 K, and the γ-to-ε phase transfomation between 100 and 200 K.

In relatively stable alloys that show no obvious anomalies, curve-fitting routines have been tried. The results indicate that theories based on thermodynamics and thermally-activated plastic flow best describe the findings for AISI 316 steels between 4 and 922 K [21-23]. In this temperature interval, the YS divides into athermal (σ_A) and thermal (σ_T) components,

$$YS = \sigma_A + \sigma_T, \quad (6)$$

where

$$\sigma_T = (\sigma_0 - \sigma_A)\exp(-CT). \quad (7)$$

Here, σ_0 is a constant, and the exponential coefficient C is a parameter related to activation energy. As shown in Fig. 3, the thermal component becomes active at 550 K (1/3 the melting point), increases exponentially at cryogenic temperatures, and emerges predominant at 4 K.

Because of the strong exponential term, plotting YS versus temperature on a semi-log scale has a linearizing effect that helps to expose subtle deviations from Eq. (7) behavior. Plotting this way in Fig. 4 reveals a remarkable variety of trends for selected steel grades. For AISI 316, no anomalous YS decreases are evident: the data trend is bilinear with inflection at 100 K [22, 23]. Other heats of AISI 316 likewise show bilinear trends, but the inflections points vary from 60 to 175 K depending on compositional variations. The inflection points correspond to changes in exponential coefficient for each heat, implying a change in deformation mechanisms takes place at these temperatures [23].

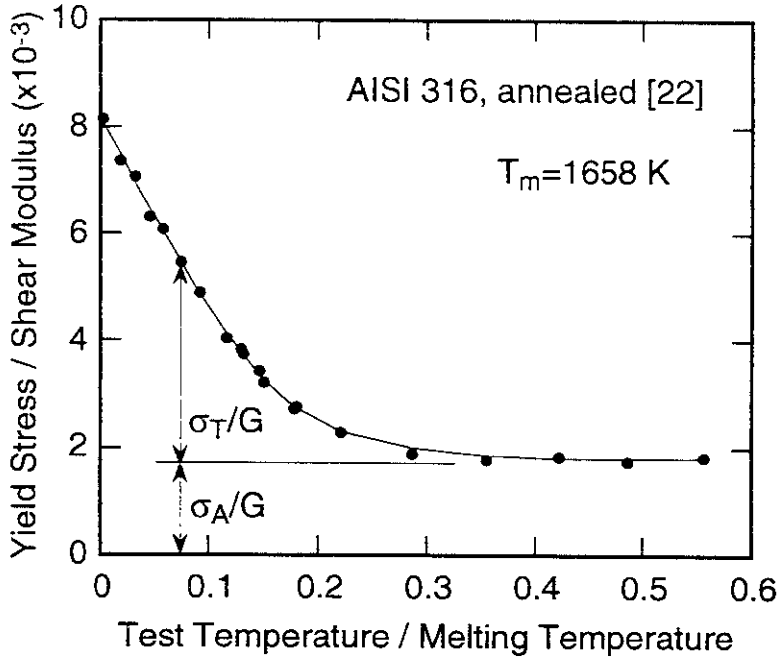

Figure 3. Thermal and Athermal Components of the YS in AISI 316 Steel.

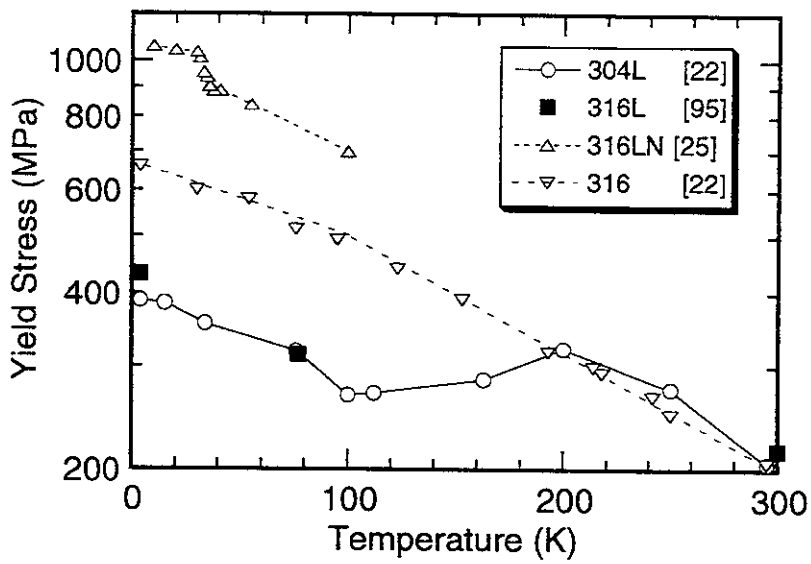

Figure 4. Anomalies in the Temperature Dependence of YS for Various Steels.

Figure 4 also shows data for an SUS 316L steel that shows little net strengthening between 300 and 77 K. Detailed data for 304L steel are included for comparison. For this 304L steel, owing to a stress-induced γ-to-ε anomaly, the YS decreases with a temperature reduction between 195 and 100 K [22]. Since the 316L and 304L data match at three points (300, 77, and 4 K), the two steels appear to behave similarly. Additional testing below 200 K might confirm the γ-to-ε anomaly for this particular heat of 316L. However, the anomaly is composition-dependent, and not all 304L and 316L grades would be equally susceptible.

Finally, data for 316LN stand in sharp contrast to the trends reported for the lower strength, (and less stable) 316L and 316 grades. Abruptly at 30 K, the 316LN shows a sudden YS increase. Obst and Bauriedl attribute this to a transition in the rate-controlling dislocation mechanisms at this temperature [25].

7. Mechanical Effects and Creep in Helium Environments

Standard tensile property measurements describe basic behavior under uniaxial loading. Such data are useful for alloy development, material selection, quality control, and structural design. However, because the response at 4 K is characterized by discontinuous yielding, the actual performance in liquid helium can be strongly influenced by mechanical or environmental factors. Special factors for magnet applications include the speed of loading, and whether load control or displacement (that is, stroke or ram) control is used. The effects of high speeds or load control are not covered in the conventional standards but are described below.

7.1 Test Speed

As the rate of mechanical loading increases, heat is generated in proportion to the rate of plastic work. The specimen temperature rises if the heat flux exceeds the cooling capacity of the cryogen. Consequently, high tensile strain rates tend to decrease the DYS and UTS compared to values measured at low strain rates, but YS is hardly affected since the source of heat evolution is mainly post-yield plastic strain.

Displacement-controlled tensile tests in liquid helium are reported for 316LN at strain rates between 10^{-5} and 10^{-2}/s [41]. As the test speed increases the UTS rises slightly but then plummets with excessive heating at strain rates greater than 2.2×10^{-3}/s. To avoid this the maximum allowable strain rate in standard tension tests (ASTM E 1450-92) is fixed at 10^{-3}/s or less.

7.2 Load Mode

In tensile tests at 4 K, the material response varies with the mode of loading. Using load control rather than conventional displacement control gives different results. In load control, discontinuous plastic elongation can be sustained for longer periods without arrest. Specimen self-heating is therefore more profuse [42, 43].

Effects of control mode on the load-carrying capability of a 316LN steel in liquid helium are shown in Fig. 5 [43]. The YS is not significantly affected by the control mode, but the EL and UTS values in load control are lower than values measured using displacement control. As the test speed in load control increases from 0.5 to 5000 N/s, the UTS falls continuously until at 5000 N/s it reaches only two-thirds the values acheived in tests of identical specimens using displacement-control.

Displacement control is traditionally used in laboratory materials tests. In such tests, the grips move apart at a fixed rate of displacement. As a result, tests in displacement-control at normal speeds display more serrations than load-controlled tests do because the plastic extensions in displacement control are machine-limited to rather small increments. The specimen heating behavior has been documented. Thermal spikes occur with each incremental extension and the specimen temperature promptly returns to 4 K when deformation is arrested. For 316-steels in displacement-control the normal relative ranking of tensile strength parameters is as shown:

$$YS < DYS < UTS. \qquad (8)$$

In load control, the applied load rate remains virtually constant, independent of material response. The stress on a cross-section tends to increase with deformation, and the increment of plastic extension is unrestricted. Depending on the material's strain hardening capability, arrests may occur infrequently. There may be only one or two instability events, in which case:

$$YS < DYS = UTS. \qquad (9)$$

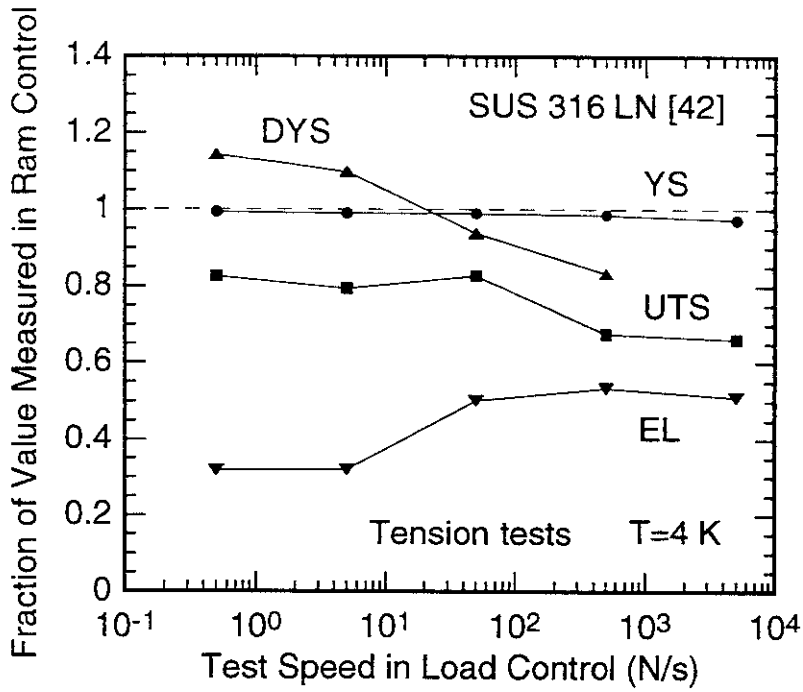

Figure 5. Load Control Effects on Tensile Property Measurements.

In other words, under tensile stress in load-control, which closely simulates magnet service conditions, sudden fracture may occur at DYS. This fact has obvious implications for design since the allowable design stress (typically set equal to one-half the UTS) for load control may be less than that for displacement control.

7.3 Creep

Creep is time-dependent strain produced by sustained static loads. Although often categorized as a high temperature phenomenon, creep occurs in metals at cryogenic temperatures at activation energies that are lower than previously expected [44]. It is now well-documented that creep occurs in 316-type steels at cryogenic temperatures. In addition to the usual steady-state creep, one instance of transient creep is reported for the case of dead-weight loading of a 316L weld at 4 K [45].

Generally, higher temperatures and stresses promote creep in the cryogenic regime. Other factors influencing creep resistance include alloy strength and work hardening rate [43]. Magnetic field effects on creep remain unstudied and unknown at the present time.

Creep rates in liquid helium have been measured for wrought 316L and 316LN steels, as well as 316L weld metal. The rates are rather low at 4 K, but larger than expected based on extrapolations of 300-K data. In 316L, stresses between 50 and 100% of the YS produce enough strain to be a factor in some magnet designs [43]. In 316L welds, the 4-K steady state creep rates are near 10^{-10}/s for applied stresses close to the YS [45]. In 316LN, creep at 4 K is not measurable unless the applied stress exceeds the YS [46]. Thus strong N-bearing grades offer superior creep resistance compared to other grades.

8. 4-K Failure Mechanisms

316-type steels that are subject to quasi-static tensile overloading at 4 K are capable of exhibiting three basic fracture mechanisms, namely: transgranular dimpled fracture, transgranular

cleavage fracture, and intergranular fracture (grain boundary decohesion). The metallurgical condition decides the predominant failure mechanism.

8.1 Ductile Fracture

The 300-series stainless steels are well known for low-temperature ductility, and ductile fracture is the preferred failure mode in primary structures. The basic features of ductile fracture are dimples created by the formation, growth, and linking of voids. Despite the crystallographic instability of the austenite phase, annealed 316-type steels characteristically show this type of fracture. Embrittlement becomes possible if other mechanisms supplant the ductile failure process.

Dimples arise from voids that typically originate at inclusions and grow with subsequent plastic strain. In wrought steels the inclusions may be MnS "stringers" (sulfide inclusion particles aligned in the rolling direction) or small spherical particles of ill-defined composition. In one commercial 316LN steel at 4 K, the failure process consisted of void nucleation and limited growth of delaminations around large MnS stringers, followed by nucleation of smaller voids in ligaments between the delaminations, causing sudden failure [47]. Single-phase castings or welds (fully austenitic structure; no ferrite) also fail in a completely ductile mode at 4 K.

Mechanical and environmental factors affect the ductile failure process by altering void nucleation and growth rates. For example, high magnetic fields can alter the average dimple size in fracture toughness tests at 4 K [62]. In sensitized steels, microvoids are able to form around precipitates in the triaxial fields (compact specimens) but not in uniaxial fields (unflawed tensile specimens) [67-68].

The dimple and inclusion densities in welds are higher compared to base metals. Microstructural studies show that the weld inclusion counts are actually lower than their dimple counts [47]. The origins of the "extra" dimples in such welds, as well as the small, secondary dimples in wrought steels [47] have not yet been traced definitively. Part of the explanation for the lack of a 1:1 correspondence in welds is that the inclusion count derives from a polished planar surface while the dimple density derives from a non-planar surface [89]. It is also feasible that small, undetectable inclusions exist, or perhaps strain concentration in austenite or at austenite-martensite interfaces provides additional initiation sites.

8.2 Brittle Fracture

Despite a record of good service histories for these steels, it is not axiomatic that high ductility and toughness must always prevail at 4 K. As shown below, the potential for cryogenic embrittlement exists for wrought products that are imperfectly processed, for heterogeneous welds, or for any sensitized steel product.

If the solution treatment temperature is incorrectly specified, the desired fully austenitic structure will not be realized in wrought steels [47]. Imperfectly processed steels may contain small amounts of nonaustenitic second phases able to impair cryogenic toughness. In fact, any steel that has a multiphase structure is likely to show a mixture of ductile and brittle failures at 4 K.

For example, in dual-phase castings and welds the ferrite phase cleaves at 4 K whereas the surrounding austenite phase remains ductile. The ferrite can dominate the fracture process if it is present in sufficient quantity or favorably distributed. The data for CF-8M castings in Fig. 6 are illustrative. As the ferrite content increases, the toughness at 4 K falls steadily and approaches a plateau value near 100 $MPa \cdot m^{1/2}$. The plateau value is nearly established when the ferrite reaches 15%, since then a continuous ferrite path is established through the ductile austenite. The toughness is then governed essentially by the fracture resistance of the ferrite alone, whereas at lower percentages of ferrite the overall toughness is some average of both austenite and ferrite [73].

Certainly the most severe form of embrittlement that can occur in these steels at 4 K is intergranular fracture (separation along the grain boundary surfaces). As discussed later,

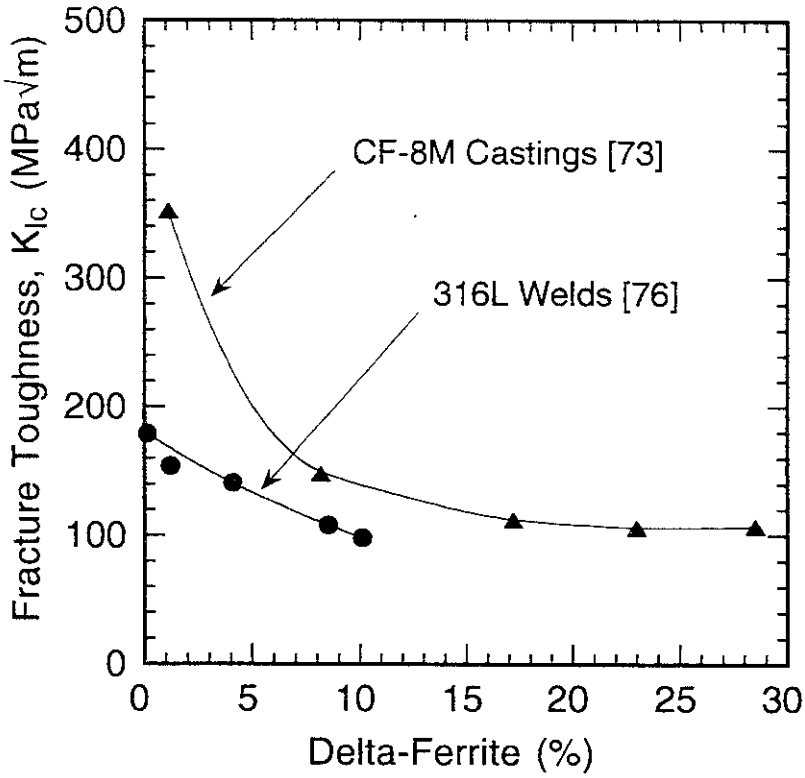

Figure 6. Effects of Ferrite on the Toughness of Castings and Welds at 4 K.

intergranular fracture is possible in any 316-type steel, casting, or weld that is sensitized by thermal aging. For instance, some 316LN conduits displayed linear breaks at 4 K with K_{Ic} in the range 60-80 MPa·$m^{1/2}$ after aging for up to 200 h at 650 or 700 °C [58, 70]. This type of fracture preempts ductile fracture at 4 K and thereby decreases the toughness to unacceptable levels. In view of the irreversible consequences, sensitization must be anticipated and avoided in magnet applications.

8.3 Transformation Effects on Fracture Behavior

The role of martensitic transformations requires some clarification. In principle, transformations can toughen or embrittle austenitic steels depending on the amounts, types, and rates of martensite formation. In 300-series steels, the published data describing empirical strength-toughness correlations for stable and unstable compositions of similar purity usually show a roughly universal trend regardless of the degree of crystallographic stability [39, 40].

Some speculate that cryogenic embrittlement is possible in these unstable steels, since α' martensite has a nonaustenitic structure. But as yet there is no compelling evidence to support the idea that newly transformed martensite embrittles the 316-type steels at 4 K. Dimpled fractures are routine in 316-type steels at 4 K, and brittle cleavage mechanisms have not been reported, despite the fact that α' forms in fractured CT specimens in large amounts up to 80%. Uniaxial tensile tests indicate that transformation does not alter the basic ductile mechanism [47], although it does influence the fracture process by promoting strain hardening. In AISI 316, the rate of strain hardening increases as soon as α' begins to form [23]. Transformations might also influence toughness by creating void initiation sites at austenite-martensite interfaces, but this effect lacks documentation.

9. **Fracture Toughness**

9.1 Cryogenic Toughness Parameters

Various parameters may be used to characterize cryogenic toughness but not all methods are equally effective at liquid helium temperature. Notched tension tests (ASTM E 602) and notched-bar impact tests (ASTM E 23) are merely qualitative, and correlations developed between them and quantitative fracture toughness parameters apparently lack the required sensitivity at 4 K [49-52].

Two fracture mechanics parameters, J_{Ic} and K_{Ic}, are used in the contemporary approach to 4-K toughness characterization. For linear elastic fractures, K_{Ic} is measured with conventional accuracy according to ASTM E 399. For ductile fractures, ASTM E 813 is used to determine a J-resistance curve, measure J_{Ic}, and estimate K_{Ic} from J_{Ic}. The variability in J-test measurements at 4 K is known from an interlaboratory study of 316LN: the average J_{Ic} measurement for 11 tests in the L-T orientation is 337 kJ/m^2, and the standard deviation is 34.4 kJ/m^2 [33-35].

The J_{Ic} test was first standardized in 1981. Subsequent revisions (1987-1989) used a different operational definition of J_{Ic}. Consequently, some bias exists when old and new data are compared. For the steel of the 4-K interlaboratory test described above, J_{Ic} in the 1987 version was 337 kJ/m^2, or 10% higher compared to the value representing the 1981 version [34]. The amount of bias varies, and is lower for lower toughness steels [53].

9.2 Metallurgical Variables

The literature documents a wide range of toughness values for the 316-type steels with greater property spreads at cryogenic temperatures. At 4 K, the lowest reported K_{Ic} is 67 MPa·m$^{1/2}$ for a severely aged 316LN containing grain boundary precipitates. The highest is 470 MPa·m$^{1/2}$ for an annealed 316LN forging. Four metallurgical factors determine the 4-K toughness of wrought and annealed products: yield strength, Ni content, inclusion content, and grain size.

For wrought steels of similar purity, the yield strength and fracture toughness values are inversely related [36, 39-40, 49]. At 4 K, the K_{Ic} estimates from J_{Ic} measurements are a monotonically decreasing function of YS as shown in Fig. 7. As austenite is strengthened it tends to lose toughness because less energy is dissipated in the fracture process, and because additional sites within the austenite matrix may nucleate voids.

Alloying effects are known from impact and fracture toughness tests. Strengthening with a sacrifice of toughness comes from adding C, N, Mo, V, or Cu. Adding Ni or eliminating S toughens without affecting strength [36]. The roles of Ni, Mo, and N have been confirmed [38], but the mechanism behind Ni's unique benefits is not yet fully understood.

High toughness is achieved by controlling the purity as well as the composition. Nonmetallic inclusions impair the ductile fracture resistance by creating easy void initiation sites. Therefore reducing the inclusion count has the beneficial effect of toughening the material without lowering the YS [36].

Based on regression analyses of data available to them, Simon and Reed [40] expressed the 4-K fracture toughness (MPa·m$^{1/2}$) of 316LN steels as a function of YS (MPa), Ni content (%), and inclusion spacing (mm):

$$K_{Ic}(J) = 150 - 0.314YS + 16.6[Ni] + 2300\lambda. \qquad (10)$$

In this equation, the inclusion spacing $\lambda = n^{-1/2}$, where n is the number of inclusions per mm^2. Cleanliness, a term implying low inclusion density or large mean inclusion spacing, is not something that can be specified in steel production, but it can be influenced by the choice of melting practice. Electroslag remelted (ESR) heats are generally superior to induction-melted heats [37, 54].

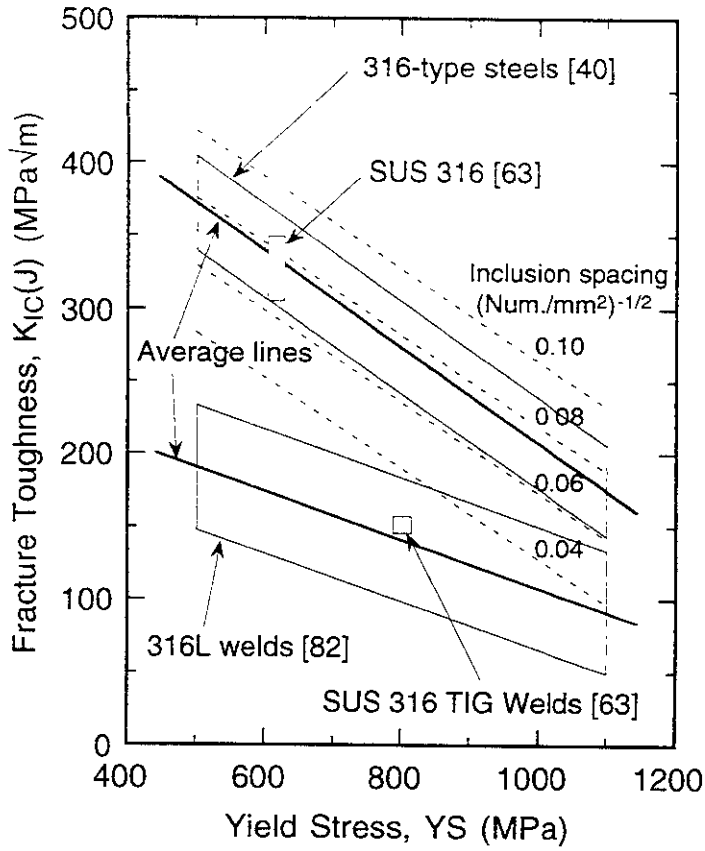

Figure 7. Strength-Toughness Relationship for 316 Steels and Welds

The strength-toughness relationship at 4 K can also be improved by grain refinement, although the grain size factor is not explicitly shown in Eq. (10). Conventional solution treatment produces plates with an average grain size of about 100 μm, whereas controlled rolling with direct quenching can reduce the grain size to between 30 and 70 μm. Thus, grain refinement has been used to advantage in manufacturing some 316LN-type steels [36,54].

9.3 Anisotropy

Fracture toughness varies with the crack-plane orientation relative to microstructural features. Therefore, in component fabrication it may be possible to increase the margin of safety by deliberately selecting a favorable orientation of stock relative to the direction of principal applied stress. To determine the degree of fracture anisotropy in a product quantitatively, thick-walled rings of forged 316LN were tested in three orthogonal orientations at 4 K [54]. The toughness ranking reported in that study is:

$$\text{C-R} > \text{C-L} > \text{L-C}. \qquad (11)$$

The toughness is higher for cracks opening under the action of hoop stresses than for cracks opening under the action of an axial (longitudinal) stress. (The first letter indicates the direction of tensile loading, the second letter gives the direction of crack propagation, and C, R, and L are the circumferencial, radial, and longitudinal directions of the cylindrical rings. See the Appendix.)

In wrought plate, the L-T orientation is typically tougher than the T-L orientation [53]. But, following a common conservative practice in the cryogenic field, the T-L orientation is routinely used for laboratory evaluations. By contrast, the T-S orientation (cracking in the through-the-thickness direction) is rarely studied. Valid K_{Ic} data for T-S orientations are essentially

nonexistent since standard compact specimens of that orientation can be extracted only from very thick products. A practical alternative for T-S orientations is the surface-cracked tension SCT test, ASTM E 740. Measurable parameters include fatigue crack growth rates and residual strengths for specimens cracked on one surface. Residual strength reflects the maximum load a cracked specimen can sustain. Such data are beginning to emerge specifically for conduits where crack growth through the wall is a relevant concern [55].

9.4 Inhomogeneity

Variations in chemistry or grain size and residual stress naturally give rise to scatter in mechanical property tests. Abnormal conditions sometimes arise during manufacture, especially in the case of thick products where processing is more difficult.

Empirical findings for 316-type steels at 4 K are mixed. A 700-mm-thick 316LN forging for MIT's Alcator C-MOD showed relatively uniform mechanical properties despite its huge size [56]. The forging was sampled at four locations, including the center and near-surface areas, using subsized tensile and compact specimens. Tests proved that the alloy chemistry was consistent throughout, and the existing grain size variations were not detrimental to the properties at 4 K.

In contrast, a 54-mm-thick wrought plate of 316LN displayed obvious irregularities including scattered toughness measurements and occasional instances of unstable fracture at 4 K. The material nonuniformity was unanticipated and frustrating to a study of specimen size effects [57]. Also, pronounced banding was discovered in a Nb-modified 316LN conduit with a 4.7 mm wall thickness. Banding is a term for microstructural stratification arising from chemical or mechanical inhomogeneities. Here the austenite grains were not equiaxed, but were elongated in the extrusion direction. The 4-K fracture was ductile, but the toughness was highly anisotropic and lower than expected. Fractography showed atypical, elongated dimples originating from rod-shaped sulfide inclusions aligned in the extrusion axis [58].

In brief, the findings suggest that while uniform properties can be obtained in some wrought 316-type steels despite extreme thickness, it is risky to assume without microstructural inspection and confirmation that any product is homogeneous. Thick welds may constitute the worst case since welds have a high potential for residual stress effects and metallurgical anisotropy.

10. Special Factors in Magnet Applications

10.1 Magnetic Fields

Like temperature, magnetic field is a relevant environmental factor that can affect the mechanical behavior of stainless steels in superconducting magnets. Theories suggest that the fracture mechanics parameters may be specifically affected. To date, only a few 316LN steels [59-62] and 316 TIG welds [63] have been tested. The empirical results are limited since experiments require unique facilities and careful attention to details of calibration.

High magnetic fields promote martensitic transformations in stainless steels. This effect has been investigated as a basic mechanism that can influence mechanical behavior. Thus, the isothermal stability of 316LN was confirmed by cooling specimens in liquid nitrogen or liquid helium, and holding for 1 h in applied magnetic fields (10 or 20 T). The amount of martensite formed was inconsequential [59]. The effects of an 8 T field on the YS of 316LN in tension at 4 K were likewise inconsequential [60].

Figure 8 summarizes the available fracture toughness data at 4 K. One study of 316LN steel shows a 20% decrease of J_{Ic} at 8 T compared to zero field [61]. A second study using another heat of 316LN shows a 23% net increase of J_{Ic} between 0 to 14.6 T. But in the second study J_{Ic} did not change monotonically. Rather, it initially decreased between 0 and 8 T, and then increased at

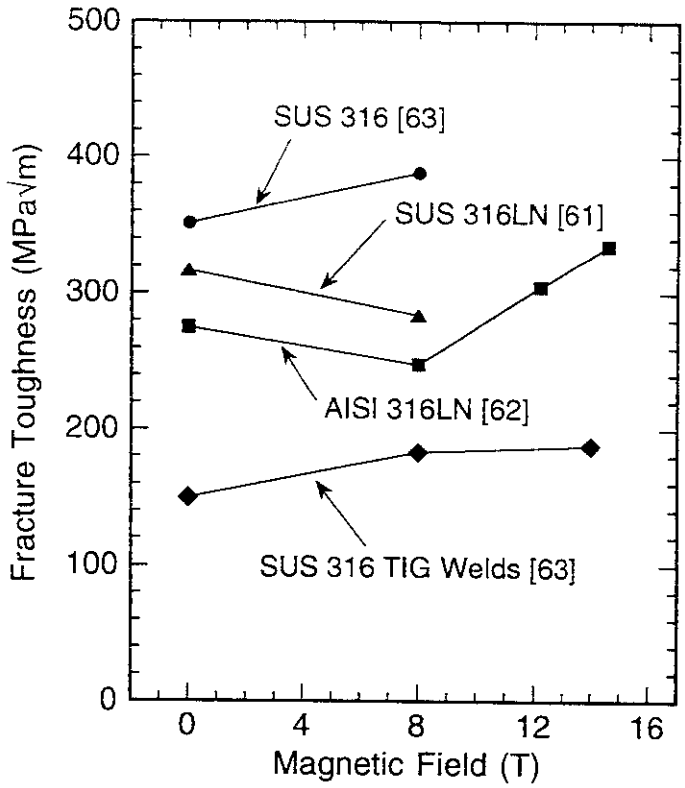

Figure 8. Magnetic Field Effects on 316LN Steels and an LHD 316 TIG Weld.

higher fields up to 14.6 T [62]. Other recent data for 316 welds indicates a slight J_{Ic} increase of no more than 10% between 0 and 13 T [63].

The limited number of tests-per-material (typically, one or two) is a weakness of the studies conducted so far. Normally, three replicate tests are recommended to define material scatter in conventional toughness tests. Therefore more data are needed to confirm the reported data trends for these and other alloys.

10.2 Size Effects

Laboratory toughness tests routinely use 25 mm thick specimens whereas fusion magnets employ a range of thicknesses from thin conduits to thick support structures. The LHD support structure is 100 mm thick for example, and coil cans in current ITER designs are thicker. Generally, size effects are accounted for if the specimen thickness is full (that is, equal in thickness to the service component). If not, size effects must be considered, especially if the laboratory specimens are thinner than the actual service components.

Textbooks predict that toughness will decrease with thickness due to a mechanical constraint imposed by geometry. Presumably, as the specimen thickness increases, crack-tip plastic deformation becomes small relative to the specimen dimensions and the measured toughness approaches a constant minimum value defined as the linear elastic plane strain fracture toughness.

At 4 K, steels thicker than 25 mm are rarely tested because the cost of facilities escalates with size. Lacking empirical data, we can make estimates using conventional size criteria as a guide to thick-section behavior. The quantity $2.5(K_{Ic}/YS)^2$ has units of thickness and is used as a criterion in test standards to gage the validity of measurements. It can also be used to predict whether a steel will show linear elastic fracture. Figure 9 shows this parameter calculated for a range of YS levels based on the strength-toughness relationships (average values) shown in Fig. 7. Comparisons between the calculated sizes for linear elastic fracture and the proposed thicknesses

for service applications suggest that linear elastic breaks can be anticipated in 316-type welds at the 100-mm thickness range, assuming the YS is 800 MPa. On the otherhand, high-strength base metals in monolithic sections are not expected to suffer linear breaks at 4 K unless the thickness exceeds about 400 mm.

As for thin components, such as conduits having tubular cross-sections and 2 to 6 mm walls, tests using full-thickness specimens are recommended. Fracture toughness data from such thin specimens will not necessarily satisfy the validity criteria of test standards. Such measurements are essentially size-dependent. Nevertheless the results are relevant for specific designs assuming that the specimen thickness is full size (the same thickness as the intended service component). Thus, size concerns are alleviated by matching the specimen and component thicknesses.

10.3 Sensitization

Major material degradation begins when stainless steels are heated in the range 450-800 °C. After sufficient time at temperature, intermetallic compounds (principally Cr carbides) precipitate in grain boundaries and (later) inside the grains as well. This precipitation creates a condition known as sensitization that can ruin corrosion resistance while reducing cryogenic ductility and toughness. Limited amounts of sensitization may be tolerated but the deterioration with continued aging is progressive; severe embrittlement at 4 K results when the precipitates become extensive enough to establish a continuous, low-energy path for cracks. A transgranular-to-intergranular fracture transition then occurs which constitutes unacceptable embrittlement.

Sensitization effects are determined by the diffusion rates of relevant elements in the steel. The primary cause of sensitization in stainless steels is C coming out of solution and forming the intermetallic compound, $M_{23}C_6$. Nitrogen comes out of solution at a slower rate, probably because of its larger atomic radius. Nevertheless, in microalloyed 316LN steels (described below) the formation of nitrides such as Cr_2N becomes an important secondary factor.

The toughness declines gradually at first and falls more abruptly as intergranular fracture begins to dominate. The aging time required to sensitize a steel is a parameter of interest that is

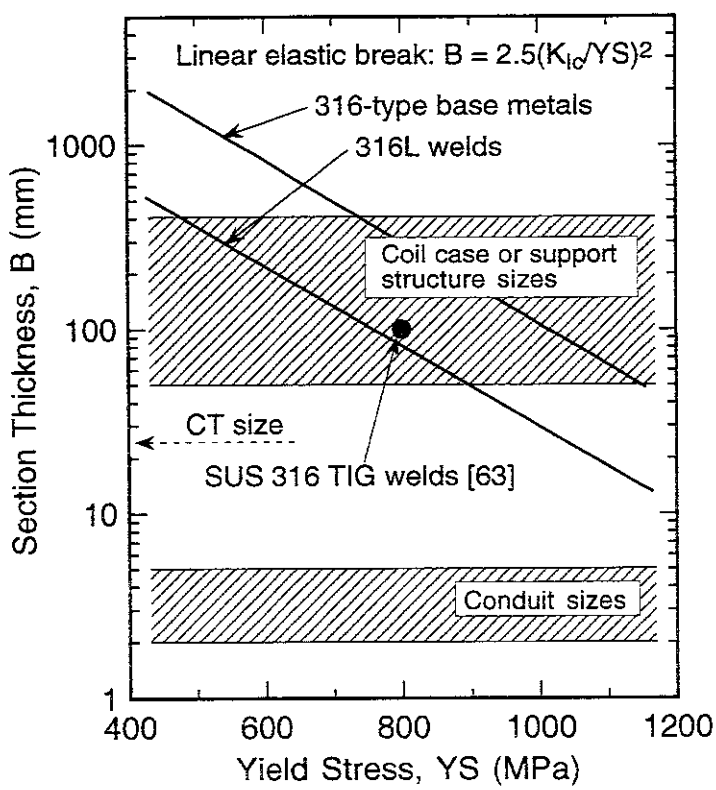

Figure 9. Thickness Effects and Size Estimates for Steels at 4 K.

fixed by the details of alloy composition, condition, and temperature. Time-temperature-sensitization curves were constructed recently to predict the aging times for some 316LN-type steels [64]. Those curves are intended to illustrate basic compositional effects and provide guidance to avoid sensitization. Because of uncertainties at this stage of knowledge, data for individual alloys must be verified before any application is made.

10.4 Aging Effects on Steel Properties

Sensitization resistance is a critical concern for wind-and-react superconductor conduits that must undergo long term thermal exposures during reaction heat treatments. In fabrication the conduits experience the Nb_3Sn reaction heat treatments that involve heating near 700 °C for 50-250 h. The exact treatment depends on the specifications for individual superconductors. The amount of cold work in the steel is also a factor. Residual cold work, about 5-20% for some conduit products, introduces dislocations that may facillitate diffusion. So steel composition and metallurgical condition must be carefully controlled to survive the thermal exposure.

The stress state of test specimens is an important factor in detecting sensitization empirically. Aging degrades the performance of cracked specimens at 4 K even though the tensile and fatigue properties of smooth hour-glass specimens may show little or no effect. Thus, aging increases the YS of 316LN at 4 K, but the effect is 10% or less [65], and it does not materialize in some microalloyed grades, nor in 316L [66-69]. Other 4-K data for 316LN indicate no measurable aging effects on S-N fatigue life despite a two-thirds drop in fracture toughness [70]. Thus, the consequences of sensitization may not be fully revealed in tests using flaw-free components or test specimens.

In view of the above, material tests to determine sensitization resistance should use specimens and procedures that simulate the expected service conditions as close as possible. Quantitative data for 316LN and modified 316LN-type steels before and after aging are shown in Table 5. Residual toughness after 180-200 h aging at 650 or 700 °C varies from 28 to 89%, depending on composition. In severely sensitized steels intergranular fracture reduces K_{Ic} to low values in the range 60 to 80 $MPa{\cdot}m^{1/2}$. Such drastic reductions can occur also in AISI 316 and 316L, but fewer quantitative data are available for those grades [69].

10.5 Preventing Sensitization

The effects of sensitization on these steels can be removed by re-annealing them at 1050 to 1100 °C, followed by rapid cooling. This restores ductility and toughness by redissolving the carbonitride precipitates and putting the C and Cr elements back into solution. Unfortunately, this

Table 5. Thermal Aging Effects on the Properties of 316LN-type Steels at 4 K.

Material Form	Ref.	Aging Treatment Time (h)/Temp (°C)	Yield Strength YS, MPa		Fracture Toughness K_{Ic}(J), $MPa{\cdot}m^{1/2}$		Retained Toughness (%)
			Before	After	Before	After	
Plate (0.019C)	[70]	200/700	1072	1135	239	67, IGF	28
Conduit (0.018C)	[58]	180/650	900	930	232	80, IGF	34
Conduit (Nb,S)	[58]	180/650	1354	1237	155	90	58
Plate (Nb,S)	[68]	200/700	1132	1125	264	167	63
Plate (Nb)	[67]	200/700	1240	1260	210	160	76
Plate (Nb,B)	[69]	200/700	1120	1120	226	202	89

(Note: All tests at 4 K; IGF = intergranular fracture; all other fractures are dimpled.)

remedy is unavailable for magnet structures after fabrication, in view of large sizeand temperature. It is therefore necessary to avoid sensitization in the first place.

The first step to improving the sensitization resistance of a steel is to minimize its C content. The specified maximum in L or LN grades is 0.03%, but levels near 0.02% are readily obtainable and should be specified. A 316LN steel with 0.018C proved useful for some NET magnet components that were aged 50 h at 680 °C [64]. However, the same steel fails intergranularly after 180 h aging at 650 °C [58]. To further extend the use of 316LN steels it appears that still lower C contents are desirable. At present, the lower limit of commercial practice is near 0.01%, but the cost, availability, and ultimate aging resistance of such a steel may be questioned. Note also that the YS would be decreased by a reduction of the C content.

Microalloying is a second way to improve aging resistance. Microalloyed 316LN grades containing Nb or V have been explored to increase the aging resistance of conduits while retaining good strength and weldability [66-69]. In combination with Nb, the effects of P, B, N, and Mo additions to 316LN were studied [67-69]. Niobium additions of about 0.05% inhibit C diffusion rates and alter the timing and type of precipitates formed. Niobium in the modified grades impedes the formation of $M_{23}C_6$ compounds, but, granted this extra time nitrides (CrNbN and Cr_2N) begin to form as well as carbides [68]. Thus, the undesirable precipitation is forestalled but not permanently prevented.

In conclusion, it appears that lowering C and microalloying offers the potential to forestall but not eliminate sensitization effects on 316 steels. The ultimate potential of sensitization-resistant Nb-alloyed steels has not yet been realized. Not every manufacturer can produce microalloyed grades efficiently or cost effectively, and further development is necessary before such products can be implemented in full scale applications.

11. Welding

Full-scale magnet construction necessitates welding which creates a heterogeneous structure with joints not usually 100% efficient. Although the 316-type steels are weldable by a variety of techniques, the wrought base metals are usually tougher than their matching 316L welds when comparisons are made at similar strengths. Design strategies emphasize locating the joints away from the most highly stressed locations, or striving to upgrade the weld properties to match the base metal performance.

Welding for extreme cryogenic service demands attention to the details of the joining process, followed by mechanical testing to confirm structural integrity. Various welding techniques may be selected depending on economic and technical factors such as joint thickness, component geometry, and accessibility of position. Significant gains in understanding have come from empirical studies using 25-mm-thick compact or bend-test specimens [92, 93]. On the otherhand, thicker welds will be required in the future, and a standard practice for weldment testing and evaluation does not exist yet.

11.1 Conventional 316L Compositions

Conventional tensile properties for welds are represented in Fig. 2. The scatterband shows the spread of YS for ten shielded metal arc weldments made using E 316L titania coated electrodes [76]. The welds in 25-mm plates were created using 17-39 passes, producing ferrite contents in the range 0.13 to 10.1%. Mechanical tests were conducted at 295, 76, and 4 K, and the envelope in the figure encompasses all measurements.

Figure 7 compares the toughness trends for several 316-type base metals and conventional welds using 316L fillers [82]. As strength increases, toughness decreases, but the welds clearly tend to relatively lower toughness. Despite the many welding processes and procedures that were used,

a sizable disparity in K_{Ic} estimates persists and the conventional welds generally fall below the base metal performance by about 40-50%.

Several approaches are available to improve the toughness of welds by developing a completely ductile fracture mechanism, and by increasing the resistance to nucleation and growth of voids which form and link to cause fracture. Contemporary research indicates this can be done by reducing or eliminating the ferrite content, reducing the inclusion content, and avoiding sensitization.

(a) Ferrite

In conventional welds intended only for room temperature service, δ-ferrite in limited amounts is desired. Ferrite prevents microfissures by inhibiting the formation of FeS and FeP (low melting point compounds) that promote hot cracking in fully austenitic welds. Microfissuring is especially prevalent in thick welds with high internal stress. Ferrite diminishes hot cracking because, compared to austenite, it has a higher solution potential for low-melting point sulfides and oxides, as well as a lower resistance to plastic deformation at higher temperatures [78].

Unfortunately, ferrite is not so desirable in welds for cryogenic service. This phase is nonaustenitic and prone to fracture by cleavage at 4 K. Moreover, decohesion owing to strain incompatibility or chemical segregation has been observed at austenite-ferrite interfaces. With respect to this behavior the effects of ferrite in welds and castings are quite similar at 4 K [73, 74].

Figure 6 demonstrates the mechanical effects of ferrite on CF-8M castings and 316L welds at 4 K. The toughness data for a controlled series of shielded metal arc SMA welds steadily decrease at ferrite contents ranging from 0 to 11% [76]. Data for a series of CF-8M castings containing 0.05N are shown for comparison. The single-phase casting (100% austenite) is capable of high toughness approaching the levels for wrought steels. It appears on the otherhand that modest amounts of ferrite severely compromise the toughness of duplex castings. In the duplex castings, increasing the ferrite or nitrogen content simultaneously raises the YS and lowers the toughness at 4 K; K_{Ic} decreases with ferrite content up to about 15% and then plateaus at 100 $MPa \cdot m^{1/2}$ [73]. Perhaps the negative role of ferrite was over-emphasized in earlier research. In practice, ferrite content is usually limited at 3-8%. At those levels, ferrite's effects may be outweighed and masked by inclusion content. Thus, a recent study indicates that the cryogenic effects of ferrite content below 7 or 8% can be perceived only when the oxygen content or inclusion content is reduced first [90].

(b) Inclusions

Another basic reason for the lower toughness of welds is their relatively high inclusion contents. The cleanliness of a deposit can be gaged by determining either the weld metal oxygen level or the inclusion density since the two are proportional [90, 92]. The plot of inclusion spacing versus a quality index parameter at 4 K shows improvements for welds and base metals alike [84]. The problem is that, compared to base metals and castings, most welds have relatively high inclusion contents owing to imperfect gas-shielding in the molten state.

Data for 19Cr-13Ni-2Mo-0.02C gas-metal arc welds clearly illustrate the effects of inclusions on cryogenic properties [89]. The inclusion count was systematically varied by changing the shielding method and gas composition. For four deposits, the inclusion count varied from 19,300 to 552,000/mm^2 whereas the 4-K YS was constant at 740 MPa. The toughness at 4 K ranged from 130 to 180 $MPa \cdot m^{1/2}$, and that spread equals the width of the scatter band for all welds in Fig. 7. In practice the inclusion count can be reduced by choice of welding process and electrode coating. The SMA process characteristically gives a relatively high inclusion content, but the amount of inclusions in SMA welds can be lowered by using electrodes with calcium-oxide-flouride coatings rather than rutile coatings [78]. The inclusion count can also be lowered by

shifting, if possible, to GMA welding. Still better results can be acheived using laser beam or electron beam welding since those techniques remelt base metal without using a filler [81, 85].

11.2 Fully Austenitic Welds

Dissimilar fillers can be used instead of the matching 316L fillers, especially if the chief goal is to develop microfissure-free single-phase austenitic structures. This is done by choice of composition and control of microstructure. If the base and weld metal compositions are dissimilar, differential thermal contraction between the base and weld metals becomes a potent factor to consider. Residual stresses arising from this source can affect microfissuring as well as mechanical property measurements.

The relative amounts of austenite and ferrite constituents in a weld deposit are controlled mainly by chemical composition. To exclude ferrite completely an appropriate chemistry is selected using the Schaeffler or DeLong diagrams. The weld is then produced with strict control over impurity elements that cause hot cracking. Experience proves it is possible to produce fissure-free austenitic welds having cryogenic properties matching the base metals [92]. The following examples emphasize the use of high Ni and Mn contents in this regard.

It is well known that nickel enhances the properties of austenitic and ferritic steels at cryogenic temperatures, at a premium on cost. This fact has been used to produce superior welds using Ni contents up to 20% [86,92]. For example, the fissure-free fully austenitic 18Cr-20Ni-5Mn-0.16N weld has 4-K properties equal to wrought steels (YS = 1015 MPa and $K_{Ic}(J) = 200$ $MPa \cdot m^{1/2}$) [86]. Manganese counteracts microfissuring while increasing the solubility of N. Up to 6% Mn may be added for these purposes. Matsumoto et al pursued this approach, producing a series of Mn-modified welds, one of which (18Cr-16Ni-6Mn-2Mo SMA butt weld) was examined in detail [87,88]. This ferrite- and fissure-free weld failed at 4 K solely by ductile mechanisms. The toughness was higher compared to conventional 316L welds, but 20% lower than wrought base metals of the same strength. Despite its completely sound austenitic microstructure, this weld did not reach full parity with base metals because of higher inclusion contents.

12. Fatigue

Fatigue is an important potential failure mode, especially in Tokamak-type magnets that operate in pulses. Since large Tokamaks can accumulate many cycles in a lifetime of operation, the fatigue resistance of some components is the design-limiting factor [5]. Fatigue crack initiation and growth in components may lead to failure by leak or by break. Leak in a superconductor conduit containing liquid helium occurs when a growing surface crack first penetrates the conduit wall. Break (catastrophic failure) occurs if the critical crack size is reached.

A 4-K fatigue database for the 316-type steels has been assembled despite the difficulties and expense of conducting experiments at this temperature. The available data include axial fatigue life for smooth specimens [70, 95-97], crack initiation lives for notched specimens [98], and fatigue crack growth rate measurements [99-105].

12.1 Smooth and Notched Specimen Results

Low-cycle fatigue data are available for annealed 316L and 316LN steels tested in fully reversed axial-strain control [70, 95]. For both steels, the fatigue life at 4 K is higher than at 295 or 77 K. High-cycle data are also available for unnotched SUS 316LN in the annealed and sensitized conditions [96]; for both conditions the conventional S-N curves shift to higher stresses at cryogenic temperatures, and the fatigue strength improvement at 10^6 cycles is proportional to the YS increase at 77 and 4 K.

Crack initiation at notch tips is reported for compact specimens of annealed AISI 316. The number of load cycles N required to generate a 0.25-mm fatigue crack is a function of the notch-tip radius, ρ, and the nominal applied stress intensity factor range, ΔK. The $\Delta K/\rho^{1/2}$-N curves are shaped like S-N curves. The crack initiation resistance improves at 76 and 4 K, and the improvement at 10^6 cycles is proportional to that of the YS [98].

12.2 Fatigue Crack Growth Rates

In large magnet structures, cracks already exist, or are assumed to exist because of inspection limitations. The service life is then determined by the rate of crack growth da/dN which correlates with ΔK, as shown schematically in Fig. 10. The da/dN-ΔK plots on logarithmic coordinates are usually subdivided into three different regimes featuring low, intermediate, and high growth rate behaviors. Long-crack, short-crack, and surface-crack data are distinguishable, and the distinctions are significant in fatigue-critical assessments of structures.

(a) Long Cracks

The growth rates of long cracks are conventionally measured using CT specimens at a fixed stress ratio, R. Experimental data are available at positive R between 0 and 0.8 which is the range of practical interest for superconducting magnets [5]. The data reported for AISI 316 at R = 0.1 are representative: The room temperature rates follow a linear trend for four orders of magnitude, whereas the 4-K curve is knee-shaped and approaches an asymptote at low ΔK [101]. At very low growth rates a threshold ΔK_T is operationally defined as the stress intensity factor corresponding to a cracking rate of 10^{-7} mm/cycle. Thresholds at this level have sometimes been estimated by extrapolations using midrange data. At 4-K, however, the experimentally determined thresholds are consistently higher than the midrange extrapolations, and, as indicated in Fig. 10, some accuracy is lost when extrapolated values are used instead of measured values.

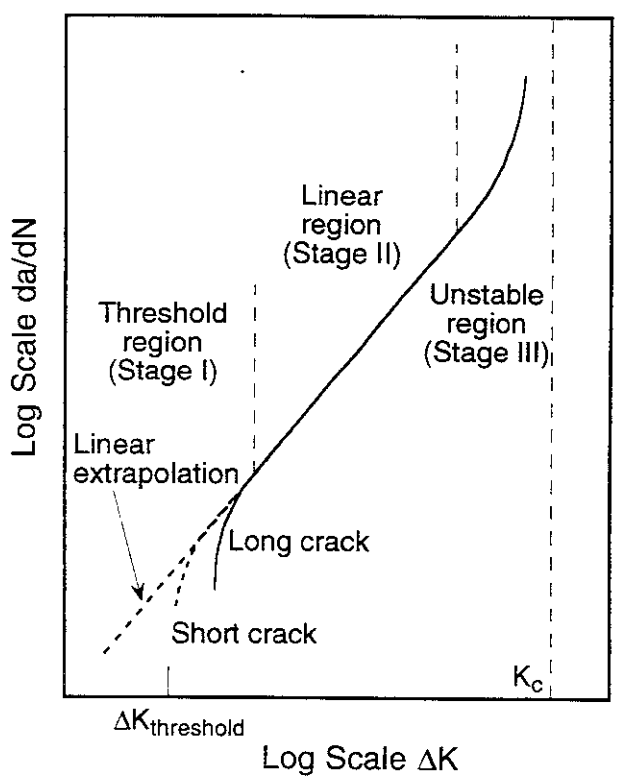

Figure 10. Fatigue Crack Growth Rates (Long Cracks at Constant R = 0.1)

Long-crack growth rate measurements such as shown in Fig. 10 are affected by crack closure. At low loads and low R ratios, certain physical processes (local plastic deformation, crack surface roughness, and volumetric expansion at crack tips due to martensitic phase trasnsformation) keep the crack closed for the initial part of the load cycle, even though the applied load may be increasing. Consequently the nominal value of ΔK overestimates the effective driving force for crack growth in this type of test. The effective or intrinsic material behavior is observed only after the closure effects are factored out. A closure correction factor may be applied to the apparent long-crack threshold.

(b) Short Cracks and Rate Simulation Test Results

Because of size effects, short cracks are exempt from closure phenomena, and they grow at higher rates than data for long-crack specimens might suggest. Conservative designs strive to account for this difference.

Short crack simulation (SCS) has been pursued at 4 K since the direct measurement of short-cracks and their growth rates is impractical at this temperature. SCS tests use compact specimens but employ a continuously increasing R-ratio that begins at 0.1 and terminates at 0.8. This procedure avoids crack closure, shortens testing time, and gives reliable cracking rates and intrinsic threshold measurements [102, 104].

Long-crack data and SCS trends for 316LN at 4 K have been compared directly [102]. Testing at R = 0.1 gives the conventional curve for long cracks where the rate measurements are subject to closure. The SCS trendline represents a relatively easy-to-measure upper bound approximation for short crack behavior. Between the two trendlines is a zone where the short-crack growth rates would be expected to fall, assuming they could be measured.

(c) Surface Cracks

Surface flaws are part-through cracks that grow simultaneously in two directions. Surface cracks are a common type of flaw in conduits and other components. Surface crack tension (SCT) tests simulate this type of crack growth better than unidirectional cracking in compact specimens can. The typical SCT specimen is a pin-loaded panel with a shallow flaw created by EDM machining. A semielliptic or semicircular crack, shaped like an actual service flaw, forms in fatigue and grows two dimensionally. By definition, a is the crack length in the through-thickness direction, and 2c is the surface crack length along the specimen width. The crack growth rate is da/dN or dc/dN, where c is half the surface crack length.

SCT data are available for two heats of 316LN at 12 K [105]. Crack growth rates dc/dN in the range 10^{-4} to 10^{-7} mm/cycle are reported for the two steel heats. The number of cycles needed to initiate a crack from an EDM flaw at R = 0.1 is a regular function of the peak fatigue stress. Fatigue in axial tension produces nearly semicircular cracks whereas fatigue in bending produces semielliptic cracks, depending on the influence of stress conditions at the vicinity of crack tips.

(d) Three Stage Behavior

In Stage III of the da/dN curve (high ΔK), an upper limit for rate measurements is encountered near 10^{-3} mm/cycle. For most 316-type steels which are ductile, the upper limit is due to the onset of excessive plastic deformation and hysteretic compliance behavior. But for some relatively brittle steels, a limit is reached because the cracking rates rapidly accelerate as K_{max} in fatigue approaches the critical value for unstable fracture. For 316-type steels, this accelerated cracking in stage III was observed for a severely sensitized 316LN conduit steel at 4 K [104].

In Stage II (midrange ΔK), the rates of cracking are governed by the power-law:

$$da/dN = C(\Delta K)^m. \quad (12)$$

Here, m is the slope of the log-log da/dN-vs-ΔK plot, and C is the value of da/dN at ΔK = 1. Some empirically determined C and m values for wrought, cast, and welded products are listed in Table 6. The value of m may depend partly on the range of stress intensity factor under consideration since the da/dN curve is not linear over wide ranges of ΔK.

Material variables can also affect the fatigue crack growth rate data. The effects depend on specific values of ΔK, and are not easy to predict. For example, midrange data for Nb-alloyed 316LN indicate that aging has little or no effect [58], or that it tends to increase C slightly compared to solution treated and quenched (STQ) material [69]. In surface-cracked 316LN alloys, rates for a cold-drawn conduit at 12 K are higher than rates for an STQ plate, and this was attributed to metallurgical differences [105].

In annealed AISI 316, test temperature which strongly affects the strength-toughness relationship had no measurable effect on the fatigue equation parameters at 295, 76, and 4 K [99]. In Stage I of the da/dN curve (low ΔK), the cracking rates diminish and approach a threshold ΔK_T below which further cracking is negligable. Threshold measurements for castings and welds are not available yet, but in wrought steels the intrinsic thresholds are higher at 4 K than at 295 K, in agreement with dislocation dynamics theory [102, 103]. Other data in Table 7 for wrought steels suggest that the near-threshold behavior at 4 K is not very microstructure-sensitive. Data exist for 316L, 316, and 316LN (plates or conduits) at selected R-ratios and temperatures (295, 76, and 4

Table 6. Midrange Fatigue Crack Growth Data Summary for 316-type Steels at 4 K.

Material & Condition	Exponent, m (-)	Coefficient, C (10^{-10} mm/cycle)	ΔK Range (MPa·$m^{1/2}$)	Reference
Wrought Steels				
annealed AISI 316	3.80	2.1	19-60	[99]
annealed AISI 316LN	3.26	7.89		[75]
annealed SUS 316L	3.96	1.2	30-60	[69]
aged	4.55	0.12	30-60	
annealed JK1S	3.96	0.9	20-60	
aged JK1S	3.69	3.5	20-60	
annealed JK1B	3.65	2.5	25-70	
aged JK1B	3.57	5	25-70	
annealed JK1P	3.81	1.4	25-70	
aged JK1P	3.75	2.6	25-70	
Castings				
CF-8M, 1% δ	3.63	2.72	23-83	[100]
CF-8M, 8% δ	3.08	34.2	23-63	[100]
CF-8M, 29% δ	3.99	1.59	20-60	[100]
Matching Welds				
316L SMA #4	3.36	1.41	30-50	[76]
316L SMA #5	3.90	1.24	20-50	
316L SMA #6	3.63	2.73	30-90	
316L SMA #7	3.95	1.09	25-90	
316L SMA #8	3.45	5.85	25-90	
Mn-modified Weld				
6%Mn SMAW	6.0	1.2×10^{-14}	26-60	[88]

K). As shown in Fig. 11, the effective or intrinsic 4-K thresholds range from 5 to 7 MPa·m$^{1/2}$, independent of variables such as YS and aging.

Table 7. Fatigue Cracking Rate Thresholds.

Temperature	Steel Type		Stress Ratio (-)	Apparent ΔK_T (MPa·m$^{1/2}$)	Closure Effect	Effective ΔK_T (MPa·m$^{1/2}$)
T = 4 K	316	[101]	0.1	8.5	2.4	6.1
	316LN	[102]	0.1	8.5	2.5	6.0
	316	[101]	0.3	6.4	1.3	5.1
	316L	[103]	0.4	6.5	0.0	6.5
	316LN	[103]	0.4	6.0	0.3	5.7
	316L	[103]	0.7	5.5	0.0	5.5
	316LN	[103]	0.7	5.2	0.0	5.2
T = 295 K	316	[101]	0.1	7.5	3.0	4.6
	316L	[103]	0.4	3.1	0.1	3.0
	316LN	[103]	0.4	3.1	0.3	2.8
	316L	[103]	0.7	2.8	0.0	2.8
	316LN	[103]	0.7	2.3	0.0	2.3

13. Discussion

13.1 Database

The cryogenic database has grown significantly in the past 20 years, but more so for base metals than for castings and welds, and more so for 316LN grades than for the 316 or 316L grades. For all grades of steels, the data spreads are larger at 4 K because metallurgical and test variables have a greater effect at cryogenic temperatures, and also because new deformation and fracture mechanisms emerge at cryogenic temperatures. The properties at 4 K can be tailored by

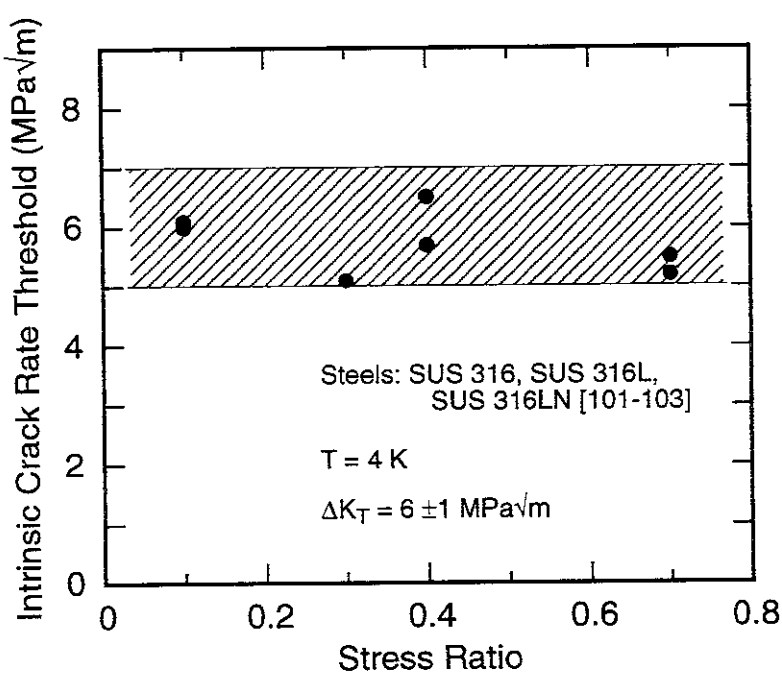

Figure 11. Intrinsic Fatigue Cracking Rate Thresholds for 316-Type Steels at 4 K.

compositional variations within the material specifications. Consequently, heat-to-heat differences at 4 K owing to chemistry variations allowed in the material specifications can be sizable. Even among different heats within a single grade, properties at 4 K can vary significantly owing to chemistry variations within the specified allowable ranges. To increase control and achieve targetted properties it may be desirable in critical cases to place more stringent requirements on specifications written for the procurement of cryogenic materials.

13.2 Uncertainty in Material Behavior

In addition to an enlarged database, understanding of structure-property relationships is needed to aid material selection and develop reliable test techniques to confirm the properties of procured materials.

Table 8 lists the predictable parameters cited in the text. These empirical predictive schemes have practical value for material selection and research purposes, but, as stated in most cases by the originators of these expressions, predicted values are not intended to be used as substitutes for empirical measurements. Discrepancies between predictions and reality are anticipated, and qualification tests are necessary before procured materials can be placed into service at 4 K.

A task in building superconducting magnets is to ensure that sufficient toughness is preserved. Cryogenic strengthening superimposed on welding and thick-section size effects tends to reduce the fracture toughness of these steels. As strength is increased, less plastic energy tends to be dissipated in ductile fractures while brittle failure mechanisms such as cleavage or intergranular fracture become more energetically favorable.

Sensitization is a potential problem for any steel that experiences high heat input. Aged superconductor conduits are a main concern because of the need for superconducrtor reaction heat treatments, but sensitization can be anticipated in any thick weld or base metal that is heated for deformation processing. Stainless steels have low thermal conductivity, and heat in thick sections cannot be dissipated quickly. Precipitation in magnet components causes irreversible damage since solution treatments to redissolve carbonitrides are not feasible in heavy-section sizes. The possibility of excessive aging must be anticipated and avoided beforehand.

Major causes of the toughness disparity between base metals and welds have been identified, but additional clarification is needed on the effects of grain structure, fracture-plane orientation, segregation, and residual stress effects, especially in thick sections.

Relatively few fatigue data exist for welds. Experience with other types of austenitic steel butt welds suggests that fatigue cracking rates may be critically dependent on crack-plane orientation relative to microstructure and residual stress [80]. Residual stress is frequently manifest in the form of high exponents ($m > 4$) in Eq. (12). Residual strength as well as fatigue crack growth rate measurements are desirable, especially for SCT tests of conduits where through-the-wall cracking can cause helium leakage. In the case of nonmatching welds, orientation and residual stress effects could outweigh other metallurgical factors.

Table 8. Parameters Predictable from Composition.

For castings:	ferrite content	FN	[12]
For welds:	ferrite content	FN	[13, 14]
For wrought steels:	Neel temperature	T_N	[15]
	Martensite start (cooling)	M_s	[10]
	Martensite start (deformation)	M_d	[11]
	4-K Yield Strength (316LN)	YS	[36, 40]
	4-K Fracture Toughness (316LN)	K_{Ic}	[40]
	Sensitization time (316LN)	t	[64]

13.3 Cryogenic Testing and Standards

Unstable plastic flow and heating at extreme cryogenic temperatures has important implications for test standards and structural design. Above 30 K, the test temperature is traditionally regarded simply as an environmental parameter that affects material properties. Below 30 K, the material response is strongly affected by the test dynamics as well as the test temperature. Therefore, some modifications to design approach appear to be justified.

(a) Tensile deformation parameters

Tensile property data in liquid helium (especially UTS and ductility measurements) lack the customary significance they have at ambient temperatures where the deformation processes are nearly isothermal and discontinuous yielding does not occur. The YS is operationally defined as an engineering measure of initial resistance to plastic deformation. At 295 K where deformation is stable, post-yield deformation requires ever-increasing loads, and ductility therefore constitutes a margin of insurance against fracture. The same margin of safety does not exist at 4 K, since plastic deformation becomes unstable.

Owing to discontinuous yielding, tensile testing in load control and displacement control produces two different material responses. Since internal heating of identically sized specimens in the two cases is different, UTS measurements in displacement control are generally not conservative compared to values acheivable in load control. Displacement control is traditionally used in laboratory materials tests, whereas load contol best simulates the service environment of many magnet structures. To simulate the 4-K service environment more precisely, it is more consistent to evaluate materials using load control.

Another approach is to forego considerations of the post-yield tensile parameters and concentrate only on the YS. Design stress levels are typically set at 1/2 the YS or 2/3 the UTS as measured in displacement controlled tests. At 4 K, the conventional YS measured at 0.2% offset is insensitive to specimen size, test speed, and mode-of-loading effects. Therefore it retains its customary significance as a reliable design parameter for magnet applications. By comparison, DYS and UTS are sensitive to many test variables; moreover, they are nonconservative, since plastic instability accompanies or precedes the stress levels they represent based on displacement-controlled standard tests.

(b) Test Procedure

In any steel susceptible to brittle fracture, the probability of failure increases at low temperatures and is greater at 4 K than at higher temperatures. Therefore tests at 77 or 295 K can not be relied upon to detect brittle behavior at 4 K [50, 75]. Tests at the 4-K service temperature are needed.

Charpy impact tests are traditionally used to detect transition temperatures in nonaustenitic steels at temperatures as low as 77 K. The standard technique of ASTM E 23-94 does not work below 77 K because it specifies no insulation. Also despite the development of improved methods, impact measurements at 4 K suffer a sensitivity loss owing to extraordinary adiabatic heating [50, 51]. Temperature rises up to 180 K are predicted and measured in stainless steel specimens during fracture at impact strain rates, and the maximum temperature rise is practically the same for any initial test temperature below 77 K [50]. Consequently, impact tests may fail to detect certain embrittlement phenomena that occur only at the most extreme cryogenic temperatures. Although recent data for alloys including 316-type steels indicate that Charpy impact tests are of limited value for screening 4-K materials, a full concensus on the limits of Charpy tests as an indicator of 4-K toughness has not yet been reached. In 316-type steels the principal sources of embrittlement are cleavage in multiphase materials containing ferrite, and intergranular fracture in severely aged

materials. Further quantitative correlations between Charpy data and K_{Ic} must be developed before the impact test could be shown to be effective in detecting embrittlement from these sources at 4 K.

14. Summary

The 316-type stainless steels are magnetically, microstructurally, and thermally unstable during mechanical tests in liquid helium. The mechanical property spreads increase at cryogenic temperatures, and are significantly greater at 4 K than at 300 K, for two basic reasons: material and test variables gain potency near absolute zero, while new deformation and fracture processes are activated. Some important trends are briefly summarized as follows:

1) The yield strength increases exponentially at cryogenic temperatures and is strongly dependent on C + N content. Strength and toughness are inversly related at 4 K.
2) The fracture toughness of 316-type steels and welds can be improved by increasing the Ni content, but many other factors tend to decrease it. Attractive strength and toughness combinations can be obtained at 4 K. However, brittle fracture is more possible at high strength levels and severe embrittlement occurs in aged steels that contain grain boundary precipitates, or in castings and welds that contain excessive inclusions or nonaustenitic phases.
3) Fatigue resistance is greater at 4 K than at room temperature. Smooth test specimens show improved life at cryogenic temperatures whereas cracked specimens show no such strength dependence. The cracking rate da/dN is critical in some applications at 4 K; complete da/dN curves exist for the base metals, but data for welds and castings are still lacking.

References

1) O. Motojima et al., Physics and Engineering Design Studies on the Large Helical Device, Fusion Eng. Des., Vol. 20, 3-14, 1993.
2) L.T. Summers, J.R. Miller, and J.R. Heim, The International Thermonuclear Experimental Reactor (ITER): Design and Materials Selection, Adv. Cryo. Eng. Maters., Vol. 36, 769-776, 1990.
3) A. Nishimura and Y. Mukai, Cold Thermal Fatigue of Austenitic Stainless Steel, Adv. Cryo. Eng. Maters., Vol. 38, 183-190, 1992.
4) A. Nishimura, H. Tamura, S. Imagawa, T. Mito, K. Takahata, J. Yamamoto, S. Mizumaki, H. Ogata, and H. Takano, Experimental Rigidity Evaluation of a Conduit Pack for Forced-Flow Superconducting Coil, Adv. Cryo. Eng. Maters., Vol. 40, 1413-1420, 1994.
5) N. Mitchell, Fatigue Assessment of the Structural Steel in Superconducting Coils for Tokamaks, Fusion Eng. Des., Vol. 19, 225-233, 1992.
6) N. Mitchell, L. Bottura, and S. Chiocchio, Safety Analysis of the Superconducting Magnet System of a Next Generation Tokamak, Fusion Eng. Des., Vol. 22, 193-216, 1993.
7) H.I. McHenry, The Properties of Austenitic Stainless Steel at Cryogenic Temperatures, in: Austenitic Steels at Low Temperatures, 1-27, Plenum, New York, 1983.
8) J.W. Morris, Jr., Structural Alloys for High Field Superconducting Magnets, Adv. Cryo. Eng. Maters., Vol. 32, 1-22, 1986.
9) S. Shimamoto, H. Nakajima, K. Yoshida, and E. Tada, Requirements for Structural Alloys for Superconducting Magnet Cases, Adv. Cryo. Eng. Maters., Vol. 32, 23-32, 1986.
10) D.C. Larbalestier and H.W. King, Prediction of Low Temperature Stability of Type 304 Stainless Steel from a Room Temperature Deformation Test, in: Proc. of the Fourth Inter. Cryo. Eng. Conf., K. Mendelssohn, ed., IPC Science and Technology Press, Guildford, Surrey, England, 338-340, 1975.

11) I. Williams, R.G. Williams, and R.C. Capellaro, Stability of Austenitic Stainless Steels Between 4 and 373 K, in: Proc. of the Sixth Int. Cryo. Eng. Conf., K. Mendelssohn, ed., IPC Science and Tech. Press, 337-341, 1976.
12) E.A. Schoefer, A One-Line Constitution Diagram for Cast Alloys, Welding Journal Res. Sup., Vol. 53, 10S, 1974.
13) A.L. Schaeffer, Constitution Diagram for Stainless Steel Weld Metal, Metal Progress, Vol. 56, 680-B, 1949.
14) W.T. DeLong, G.A. Ostrom, and E.R. Szumachowski, Measure and Calculation of Ferrite in Stainless Steel Weld Metal, Welding Journal, Vol. 35, 521s-528s, 1956.
15) L.A. Warnes and H.W. King, The Low Temperature Magnetic Properties of Austenitic Fe-Cr-Ni Alloys 2. The Prediction of Neel Temperatures and Maximum Susceptibilities, Cryogenics, Vol. 16, 659-667, 1976.
16) E.W. Collings, The Magnetic Character of Austenitic Stainless Steels, Adv. Cryo. Eng. Maters., Vol. 26, 37-47, 1980.
17) E.W. Collings and S.C. Hart, Low Temperature Magnetic Susceptibility and Magnetization Studies of Some Commercial Stainless Steels, Cryogenics, Vol. 19, 521-530, 1979.
18) H.M. Ledbetter and E.W. Collings, Low Temperature Magnetic and Elastic Constant Anomalies in Three Manganese Stainless Steels, in: Metal Science of Stainless Steels, Metal. Soc. AIME, New York, 22-38, 1978.
19) H.M. Ledbetter, Stainless Steel Elastic Constants at Low Temperatures, J. Appl. Phys., Vol. 52, 1587-1589, 1981.
20) H.M. Ledbetter, Austenitic-Steel Elastic Constants, in: Austenitic Steels at Low Temperature, 83-101, Plenum, New York, 1983.
21) G.P. Sanderson and and D.T. Llewellyn, Mechanical Properties of Standard Austenitic Stainless Steels in the Temperature Range -196 to + 800 °C, J. Iron Steel Inst., Vol. 207, 1129-1140, 1969.
22) R.L. Tobler, R.P. Reed, and D.S. Burkhalter, Temperature Dependence of Yielding in Austenitic Stainless Steels, Adv. Cryo. Eng., Vol. 26, 107-119, 1980.
23) R.L. Tobler, D.H. Beekman, and R.P. Reed, Factors Influencing the Low Temperature Dependence of Yielding in AISI 316 Stainless Steels, in: Austenitic Stainless Steels at Low Temperature, Plenum, New York, 135-167, 1983.
24) B. Obst and D. Pattanayak, Discontinuous Deformation Modes of a Nitrogen-Stabilized Austenitic Steel, Adv. Cryo. Eng. Maters., Vol. 28, 57-65, 1982.
25) B. Obst and W. Bauriedl, The Instability of Plastic Flow at Low Temperatures - An Explanation from a New Point of View, Adv. Cryo. Eng. Maters., Vol. 34, 275-282, 1988.
26) V.Y. Ilyichev, Y.M. Medvedev, I.A. Shapovaliev, and I.N. Klimenko, The Low Temperature Anomaly of the Temperature Dependence of the Flow Stresses in Fe-Cr-Ni Alloys, Phys. Met. Metall., Vol. 44, 173-176, 1978.
27) B.I. Verkin, Y.A. Ilyichev, I.M. Klimenko, The Low Temperature Change of the Magnetic Structure and Plastic Properties of Fe-Cr-Ni Alloys, Adv. Cryo. Eng., Vol. 26, 120-125, 1980.
28) K.A. Yushchenko, B.I. Verkin, V.Y. Ilichev, and I.N. Klimenko, The Influence of Magnetic Structure on Temperature Dependence of the Yield Strength of 20Cr-16Ni-6Mn Steel at Low Temperatures, Adv. Cryo. Eng. Maters., Vol. 28, 67-72, 1982.
29) R.P. Reed, R.L. Tobler, and J.W. Elmer, Temperature Dependence of Flow Strength of Selected Austenitic Stainless Steels, in: Austenitic Steels at Low Temperature, Plenum, New York, 105-116, 1983.
30) G.Y. Chin, W.F. Hosford, Jr., and W.A. Backofen, Influence of the Mechanical Loading System on Low-Temperature Plastic Instability, Trans. AIME, Vol. 230, 1043-1048, 1964.
31) D.T. Read and R.P. Reed, Heating Effects During Tensile Tests of 304L Stainless Steel at 4 K, Adv. Cryo. Eng. Maters., Vol. 26, 91-101, 1980.
32) R.P. Reed and N.J. Simon, Discontinuous Yielding During Tensile Tests at Low Temperature, Adv. Cryo. Eng. Maters., Vol. 36, 1077-1086, 1990.

33) T. Ogata, K. Nagai, K. Ishikawa, K. Shibata, and E. Fukushima, VAMAS Interlaboratory Fracture Toughness Test at Liquid Helium Temperature, Adv. Cryo. Eng. Maters., Vol. 36, 1053-1060, 1990.
34) T. Ogata, K. Nagai, K. Ishikawa, K. Shibata, and S. Murase, VAMAS Second Round Robin Tests of Structural Materials at Liquid Helium Temperature, Adv. Cryo. Eng. Maters., Vol. 38, 69-76, 1992.
35) T. Ogata, K. Nagai, and K. Ishikawa, VAMAS Tests of Structural Materials at Liquid Helium Temperature, Adv. Cryo. Eng. Maters., Vol. 40, 1191-1198, 1994.
36) S. Yamamoto, N. Yamagami, and C. Ouchi, Effect of Metallurgical Variables on the Strength and Toughness of Mn-Cr and Ni-Cr Stainless Steels at 4.2 K, Adv. Cryo. Eng. Maters., Vol. 32, 57-64, 1986.
37) Y. Takahashi, K. Yoshida, M. Shimada, E. Tada, R. Miura, and S. Shimamoto, Mechanical Evaluation of Nitrogen-Strengthened Stainless Steels at 4 K, Adv. Cryo. Eng. Maters., Vol. 28, 73-81, 1982.
38) P.T. Purtscher, R.P. Walsh, and R.P. Reed, Effect of Chemical Composition on the 4-K Mechanical Properties of 316LN-Type Alloys, Adv. Cryo. Eng. Maters., Vol. 34, 191-198, 1988.
39) N.J. Simon and R.P. Reed, Strength and Toughness of AISI 304 and 316 at 4 K, J. Nuclear Maters., Vol. 141-143, 44-48, 1986.
40) N.J. Simon and R.P. Reed, Design of 316LN-Type Alloys, Adv. Cryo. Eng. Maters., Vol. 34, 165-172, 1988.
41) R.P. Reed and R.P. Walsh, Tensile Strain Rate Effects in Liquid Helium, Adv. Cryo. Eng. Maters., Vol. 34, 199-208, 1988.
42) T. Ogata, K. Ishikawa, R.P. Reed, and R.P. Walsh, Loading Rate Effects on Discontinuous Deformation in Load Control Tensile Tests, Adv. Cryo. Eng. Maters, Vol. 34, 233-241, 1988.
43) T. Ogata and K. Ishikawa, Time Dependent Deformation of Austenitic Stainless Steels at Cryogenic Temperatures, Cryogenics, Vol. 26, 365-369, 1986.
44) J.K. Tien and C.T. Yen, Cryogenic Creep of Metals, Adv. Cryo. Eng. Maters., Vol. 30, 319-338, 1984.
45) L. D. Roth, A.E. Manhart, E.N.C. Dalder, and R.P. Kershaw, Jr., Creep of 304LN and 316 L Stainless Steels at Cryogenic Temperatures, Adv. Cryo. Eng. Maters., Vol. 32, 369-376, 1986.
46) T. Ogata, O. Umezawa, and K. Ishikawa, Low Temperature Creep Behavior of Stainless Steels, Adv. Cryo. Eng. Maters., Vol. 36, 1233-1239, 1990.
47) P.T. Purtscher R.P. Walsh, and R.P. Reed, Fracture Behavior of 316LN Alloy in Uniaxial Tension At Cryogenic Temperatures, Adv. Cryo. Eng. Maters., Vol. 34, 379-386, 1988.
48) D.T. Read and R.P. Reed, Fracture and Strength Properties of Selected Austenitic Stainless Steels at Cryogenic Temperatures, Cryogenics, Vol. 21, 415-417, 1981.
49) R.P. Reed, D.T. Read, and R.L. Tobler, Notch Tensile Measurements and Fracture Toughness Correlations For Austenitic Stainless Steels, Adv. Cryo. Eng. Maters., Vol. 32, 361-368, 1986.
50) I.S. Hwang, M.M. Morra, R.G. Ballinger, H. Nakajima, and R.L. Tobler, Charpy Absorbed Energy and JIc as Measures of Cryogenic Fracture Toughness, J. Test. Eval., Vol. 20, 248-258, 1992.
51) H. Nakajima, K. Yoshida, H. Tsuji, R.L. Tobler, I.S. Hwang, M.M. Morra, and R.G. Ballinger, The Charpy Impact Test as an Evaluation of 4-K Fracture Toughness, Adv. Cryo. Eng. Maters., Vol. 38, 207-215, 1992.
52) J. Kubler, H.J. Schindler, and W. J. Muster, Influence of Aging on the Fracture Toughness of Cryogenic Austenitic Materials Evaluated by a Simple Test Method, Adv. Cryo. Eng. Maters., Vol. 38, 191-198, 1992.
53) Y.A. Rosenthal, R.L. Tobler, and P.T. Purtscher, JIc Data Analysis Methods with a Negative Crack Growth Correction Procedure, J. Test. Eval., Vol. 18, 301-304, 1990.

54) H. Krauth and A. Nyilas, Toughness and Fatigue Properties of Austenitic Steels at Cryogenic Temperature and Their Application in Complex Structures, in: Austenitic Steels at Low Temperatures, 159-169, Plenum, New York, 1983.
55) A. Nyilas, B. Obst, and A. Ulbricht, Simulations on Jacket Material Failure of Net-Superconductors by Surface Crack Growth in 316LN Type Materials at 12 K, Adv. Cryo. Eng. Maters., Vol. 40, 1239-1246, 1994.
56) E.S. Drexler, N.J. Simon, and R.P. Reed, Strength and Toughness at 4 K of Forged Heavy-Section 316LN, Adv. Cryo. Eng. Maters., Vol. 40, 1199-1206, 1994.
57) T. Ogata, K. Ishikawa, T. Yuri, R.L. Tobler, P.T. Purtscher, R.P. Reed, T. Shoji, K. Nakano, and H. Takahshi, Effects of Specimen Size, Side-Grooving, and Precracking Temperature on J-integral Test Results for AISI 316LN at 4 K, Adv. Cryo. Eng. Maters., Vol. 34, 259-266, 1988.
58) R.L. Tobler, R.P. Walsh, C.N. McCowan, and R.P. Reed, Mechanical Properties of a Superconductor Conduit Proposed for ITER Magnets, presented at: Third International Toki Conference, Applied Superconductivity for Fusion Nuclear Research, Dec. 3-5, 1991, Toki, Japan.
59) K. Shibata, Y. Kurita, T. Shimonosono, Y. Murakami, S. Awaji, and K. Watanabe, Effects of High Magnetic Fields on Martensitic Transformation at Cryogenic Temperatures for Variously Heat Treated Stainless Steels, Adv. Cryo. Eng. Maters., Vol. 40, 1207-1213, 1994.
60) Y. Kurita, T. Shimonosono, and K. Shibata, Effects of an 8 Tesla Magnetic Field on Tensile Deformation of Stainless Steels at 4 K, Adv. Cryo. Eng. Maters., Vol. 40, 1223-1229, 1994.
61) S. Murase, S. Kobatake, M. Tanaka, I. Tashiro, O. Horigami, H. Ogiwara, K. Shibata, K. Nagai, and K. Ishikawa, Effects of a High Magnetic Field on the Fracture Toughness at 4.2 K for Austenitic Stainless Steels, Fusion Eng. Des., Vol. 20, 451-454, 1993.
62) J.W. Chan, D. Chu, C. Tseng, and J.W. Morris, Jr., Cryogenic Fracture Behavior of 316LN in Magnetic Fields Up to 14.6 T, Adv. Cryo. Eng. Maters., Vol. 40, 1215-1221, 1994.
63) A. Nishimura, J. Yamamoto, O. Motojima, J.W. Chan, J.W. Morris, Jr., R.L. Tobler, H. Takahashi, and S. Suzuki, Fracture Toughness of Partially Welded Joints of SUS 316 in High Magnetic Field at 4 K, in press, Adv. Cryo. Eng. Maters., Vol. 42, Plenum (to be published).
64) W.J. Muster and J. Elster, Low Temperature Embrittlement After Aging Stainless Steels, Cryogenics, Vol. 30, 799-802, 1990.
65) R.P. Reed, R.P. Walsh, and C.N. McCowan, Effects of Nb3Sn Heat Treatment on the Strength and Toughness of 316LN Alloys with Different Carbon Contents, Adv. Cryo. Eng. Maters., Vol. 38, 45-54, 1992.
66) K. Nohara, T. Kato, T. Sasaki, S. Suzuki, and Y. Ono, Cryogenic Properties of Austenitic Stainless Steels for Superconducting Magnet, in: Austenitic Steels at Low Temperatures, 117-133, Plenum, New York, 1983.
67) M. Shimada and S. Tone, Effects of Niobium on Cryogenic Mechanical Properties of Aged Stainless Steels, Adv. Cryo. Eng. Maters., Vol. 34, 131-139, 1988.
68) M. Shimada, Cryogenic Mechanical Properties of an Aged Austenitic Stainless Steel, Fusion Eng. Des., Vol. 20, 437-443, 1993.
69) M. Shimada, Fatigue Crack Growth Rate at 4 K of Aged Austenitic Stainless Steels, Adv. Cryo. Eng. Maters., Vol. 36, 1217-1224, 1990.
70) T. Ogata, K. Ishikawa, K. Nagai, O. Umezawa, and T. Yuri, Low Cycle Fatigue and Other Mechanical Properties of Aged 316LN Stainless Steel at Liquid Helium Temperature, Adv. Cryo. Eng. Maters., Vol. 36, 1249-1255, 1990.
71) D. Dew-Hughes and K.S. Lee, The Choice of Steel for the Isabelle Magnet Tubes, Adv. Cryo. Eng. Maters., Vol. 26, 151-157, 1981.
72). K.S. Lee and D. Dew-Hughes, The Effect of -Ferrite upon the Low Temperature Mechanical Properties of Centrifugally Cast Stainless Steels, in: Austenitic Steels at Low Temperatures, 221-242, Plenum, New York, 1983.
73) T.A. Whipple and H.I. McHenry, The Mechanical Properties of Stainless Steel Castings at 4 K, in: Austenitic Steels at Low Temperatures, 243-248, Plenum, New York, 1983.

74) E L. Brown, T.A. Whipple, and R.L. Tobler, Fracture Toughness of CF8 Castings at Four Kelvin, Metall. Trans., Vol. 14A, 1179-1188, 1983.
75) F N. Mazandarany, D.M Parker, R.F. Koenig, and D.T. Read, A Nitrogen-Strengthened Austenitic Stainless Steel for Cryogenic Magnet Structures, Adv Cryo. Eng. Maters., Vol. 26, 158-169, 1980.
76) D.T. Read, H.I. McHenry, P.A. Steinmeyer, and R.D. Thomas, Jr., Metallurgical Factors Affecting the Toughness of 316L SMA Weldments at Cryogenic Temperatures, Weld. J., Vol. 59, 104-113s, 1980.
77) T.A. Whipple, H.I. McHenry, and D.T. Read, Fracture Behavior of Ferrite Free Stainless Steel Welds in Liquid Helium, Weld. J., Vol. 60, 72s-78s, 1981.
78) A. Nyilas and H. Krauth, Use of Heavy Section Austenitic Welds for 4-K Service, Adv. Cryo. Eng. Maters., Vol. 28, 853-863, 1982.
79) E.N.C. Dalder, O.W. Seth, and T.A. Whipple, Shielded Metal-Arc and Flux-Cored Metal-Arc Stainless Steel Weldments: Magnet Cases for 4-K Service, Adv. Cryo. Eng. Maters., Vol. 28, 839-851, 1982.
80) R.L. Tobler, H.I. McHenry, and R.P. Reed, Fracture Mechanics Parameters for an Iron-13%Cr-19%Mn Stainless Steel and Its Welds at Cryogenic Temperatures, in: Adv. Cryo. Eng. Maters., Vol. 24, 460-472, 1978.
81) T. Ogata, K. Nagai, K. Hiraga, K. Ishikawa, and H. Irie, Effect of EB-Weld and Cold-Rolling on Low Temperature Strength and Toughness of Austenitic Stainless Steels, in: Austenitic Steels at Low Temperatures, 211-220, Plenum, New York, 1983.
82) R.L. Tobler, T.A. Siewert, and H.I. McHenry, Strength-Toughness Relationship for Austenitic Stainless Steel Welds at 4 K, Cryogenics, Vol. 26, 392-395, 1986.
83) C.N. McCowan, T.A. Siewert, R.P. Reed, and F.B. Lake, Manganese and Nitrogen in Stainless Steel SMA Welds for Cryogenic Service, Weld. J., Vol. 66, 84s, 1987.
84) C.N. McCowan and T.A. Siewert, Inclusions and Fracture Toughness in Stainless Steel Welds at 4 K, Adv. Cryo. Eng. Maters., Vol. 34, 335-342, 1988.
85) T.A. Siewert, D. Gorni, and G. Kohn, High-Energy-Beam Welding of Type 316LN Stainless Steel for Cryogenic Applications, Adv. Cryo. Eng. Maters., Vol. 34, 343-350, 1988.
86) C.N. McCowan, T.A. Siewert, and R.L. Tobler, Tensile and Fracture Properties of an Fe-18Cr-20Ni-5Mn-0.16N Fully Austenitic Weld Metal at 4 K, J. Eng. Maters. Tech., Vol. 108, 340-343, 1986.
87) T. Matsumoto, H. Satoh, Y. Wadayama, and F. Hataya, Mechanical Properties of Fully Austenitic Weld Deposits for Cryogenic Structures, Weld. Res. Supplement, Vol. 66, 120s-126s, 1987.
88) R.L. Tobler, R.E. Trevisan, T.A. Siewert, H.I. McHenry, P.T. Purtscher, R.P. Reed, C.N. McCowan, and T. Matsumoto, Strength, Fatigue, and Toughness Properties of an Fe-18Cr-16Ni-6Mn-2Mo Fully Austenitic SMA Weld at 4 K, Adv. Cryo. Eng. Maters., Vol. 34, 351-358, 1988.
89) C.N. McCowan and T.A. Siewert, Fracture Toughness of 316L Stainless Steel Welds with Varying Inclusion Contents at 4 K, Adv. Cryo. Eng. Maters., Vol. 36, 1331-1337, 1990.
90) J.H. Kim, B.W. Oh, J.G. Youn, G.W. Bahng, and H.M. Lee, Effect of Oxygen Content On Cryogenic Toughness of Austenitic Stainless Steel Weld Metal, Adv. Cryo. Eng. Maters., Vol. 36, 1339-1346, 1990.
91) D.J. Alexander and G.M. Goodwin, Thick-Section Weldments in 21-6-9 and 316LN Stainless Steels for Fusion Energy Applications, Adv. Cryo. Eng. Maters., Vol. 38, 101-107, 1992.
92) T.A. Siewert and C.N. McCowan, Joining of Austenitic Stainless Steels for Cryogenic Applications, Adv. Cryo. Eng. Maters., Vol. 38, 109-114, 1992.
93) A. Nishimura, The Use of Cryogenic Structural Steels and Their Welding and Joining, Cryo. Eng., Vol. 26, 167-175, 1991.
94) K. Nagai, T. Yuri, O. Umezawa, T. Ogata, K. Ishikawa, High Cycle Fatigue Properties of Cryogenic Structural Alloys, Cryo. Eng., Vol. 26, 255-262, 1991.

95) K. Suzuki, F. Fukakura, and H. Kashiwaya, Cryogenic Fatigue Properties of 304L and 316L Stainless Steels Compared to Mechanical Strength and Increasing Magnetic Permeability, J. Test. Eval., Vol. 16, 191-197, 1988.
96) O. Umezawa, T. Ogata, T. Yuri, K. Nagai, and K. Ishikawa, Review of High Cycle Fatigue Properties of Structural Materials at Cryogenic Temperatures, Adv. Cryo. Eng. Maters., Vol. 40, 1231-1237, 1994.
97) K. Ishikawa, T. Yuri, O. Umezawa, K. Nagai, and T. Ogata, Fatigue Testing and Properties of Structural Materials at Cryogenic Temperatures, Fusion Eng. Des., Vol. 20, 429-435, 1993.
98) R.L. Tobler and Q.S. Shu, Fatigue Crack Initiation from Notches in Austenitic Stainless Steels, Cryogenics, Vol. 26, 396-401, 1986.
99) R.L. Tobler, and R.P. Reed, Fatigue Crack Growth Resistance of Structural Alloys at Cryogenic Temperatures, Adv. Cryo. Eng., Vol. 24, 82-90, 1978.
100) P.T. Purtscher, Y.W. Cheng, and P.N. Li, Fatigue Crack Growth of Duplex Stainless Steel Castings at 4 K, J. Eng. Maters. Tech., Vol. 107, 161-165, 1985.
101) R.L. Tobler, Near Threshold Fatigue Crack Growth Behavior of AISI 316 Stainless Steel, Adv. Cryo. Eng. Maters., Vol. 32, 321-327, 1986.
102) R.L. Tobler, J.R. Berger, and A. Bussiba, Long Crack Fatigue Thresholds and Short Crack Simulation at Liquid Helium Temperature, Adv. Cryo. Eng. Maters., Vol. 38, 159-166, 1992.
103) K. Suzuki, J. Fukakura, and H. Kashiwaya, Near-Threshold Fatigue Crack Growth of Austenitic Stainless Steels at Liquid Helium Temperature, Adv. Cryo. Eng. Maters., Vol. 38, 149-158, 1992.
104) A. Bussiba, R.L. Tobler, and J.R. Berger, Superconductor Conduits: Fatigue Crack Growth Rate and Near-Threshold Behavior of Three Alloys, Adv. Cryo. Eng. Maters., Vol. 38, 167-174, 1992.
105) A. Nyilas, J. Zhang, B. Obst, and A. Ulbricht, Fatigue and Fatigue Crack Growth Properties of 316LN and Incoloy 908 Below 10 K, Adv. Cryo. Eng. Maters., Vol. 38, 133-140, 1992.

APPENDIX

DESIGNATIONS FOR CRACK PLANE ORIENTATIONS

I. Base Metal

For unwelded base metals, the fracture plane orientation is designated using a two-letter code. The first letter desginates the direction normal to the crack plane. The second denotes the expected direction of crack propagation.

For rectangular products (Wrought Plate):

L = Longitudinal or principal forming direction (maximum grain flow)
T = Transvers direction
S = Short transverse direction or third orthogonal direction.

For Cylindrical Products:

L = longitudnal axis
R = radial direction
C = circumferential or tangential direction

II. Weldments

For weldments, a three letter code is used. The first letter designates the direction normal to the crack plane, and the second designates the expected direction of crack growth; the third letter is the crack tip location.

W = the direction of welding.
T or L is the rolling direction of the plate.

The most commonly tested crack plane orientations are the TW or LW and TS or LS. Because of material limitations, bend bars are commonly used whereas compact specimens are routinely used for base metals.

Recent Issues of NIFS Series

NIFS-385 H. Kitabata, T. Hayashi, T. Sato and Complexity Simulation Group,
Impulsive Nature in Collisional Driven Reconnection; Nov. 1995

NIFS-386 Y. Katoh, T. Muroga, A. Kohyama, R.E. Stoller, C. Namba and O. Motojima,
Rate Theory Modeling of Defect Evolution under Cascade Damage Conditions:The Influence of Vacancy-type Cascade Remnants and Application to the Defect Production Chracterization by Microstructural Analysis; Nov. 1995

NIFS-387 K. Araki, S. Yanase and J. Mizushima,
Symmetry Breaking by Differential Rotation and Saddle-node Bifurcation of the Thermal Convection in a Spherical Shell; Dec. 1995

NIFS-388 V.D. Pustovitov,
Control of Pfirsch-Schlüter Current by External Poloidal Magnetic Field in Conventional Stellarators: Dec. 1995

NIFS-389 K. Akaishi,
On the Outgassing Rate Versus Time Characteristics in the Pump-down of an Unbaked Vacuum System; Dec. 1995

NIFS-390 K.N. Sato, S. Murakami, N. Nakajima, K. Itoh,
Possibility of Simulation Experiments for Fast Particle Physics in Large Helical Device (LHD); Dec. 1995

NIFS-391 W.X.Wang, M. Okamoto, N. Nakajima, S. Murakami and N. Ohyabu,
A Monte Carlo Simulation Model for the Steady-State Plasma in the Scrape-off Layer; Dec. 1995

NIFS-392 Shao-ping Zhu, R. Horiuchi, T. Sato and The Complexity Simulation Group,
Self-organization Process of a Magnetohydrodynamic Plasma in the Presence of Thermal Conduction; Dec. 1995

NIFS-393 M. Ozaki, T. Sato, R. Horiuchi and the Complexity Simulation Group
Electromagnetic Instability and Anomalous Resistivity in a Magnetic Neutral Sheet; Dec. 1995

NIFS-394 K. Itoh, S.-I Itoh, M. Yagi and A. Fukuyama,
Subcritical Excitation of Plasma Turbulence; Jan. 1996

NIFS-395 H. Sugama and M. Okamoto, W. Horton and M. Wakatani,
Transport Processes and Entropy Production in Toroidal Plasmas with Gyrokinetic Eletromagnetic Turbulence; Jan. 1996

NIFS-396 T. Kato, T. Fujiwara and Y. Hanaoka,
X-ray Spectral Analysis of Yohkoh BCS Data on Sep. 6 1992 Flares

- Blue Shift Component and Ion Abundances -; Feb. 1996

NIFS-397 H. Kuramoto, N. Hiraki, S. Moriyama, K. Toi, K. Sato, K. Narihara, A. Ejiri, T. Seki and JIPP T-IIU Group,
Measurement of the Poloidal Magnetic Field Profile with High Time Resolution Zeeman Polarimeter in the JIPP T-IIU Tokamak; Feb. 1996

NIFS-398 J.F. Wang, T. Amano, Y. Ogawa, N. Inoue,
Simulation of Burning Plasma Dynamics in ITER; Feb. 1996

NIFS-399 K. Itoh, S-I. Itoh, A. Fukuyama and M. Yagi,
Theory of Self-Sustained Turbulence in Confined Plasmas; Feb. 1996

NIFS-400 J. Uramoto,
A Detection Method of Negative Pionlike Particles from a H2 Gas Descharge Plasma; Feb. 1996

NIFS-401 K.Ida, J.Xu, K.N.Sato, H.Sakakita and JIPP TII-U group,
Fast Charge Exchange Spectroscopy Using a Fabry-Perot Spectrometer in the JIPP TII-U Tokamak; Feb. 1996

NIFS-402 T. Amano,
Passive Shut-Down of ITER Plasma by Be Evaporation; Feb. 1996

NIFS-403 K. Orito,
A New Variable Transformation Technique for the Nonlinear Drift Vortex; Feb. 1996

NIFS-404 T. Oike, K. Kitachi, S. Ohdachi, K. Toi, S. Sakakibara, S. Morita, T. Morisaki, H. Suzuki, S. Okamura, K. Matsuoka and CHS group; *Measurement of Magnetic Field Fluctuations near Plasma Edge with Movable Magnetic Probe Array in the CHS Heliotron/Torsatron*; Mar. 1996

NIFS-405 S.K. Guharay, K. Tsumori, M. Hamabe, Y. Takeiri, O. Kaneko, T. Kuroda,
Simple Emittance Measurement of H- Beams from a Large Plasma Source; Mar. 1996

NIFS-406 M. Tanaka and D. Biskamp,
Symmetry-Breaking due to Parallel Electron Motion and Resultant Scaling in Collisionless Magnetic Reconnection; Mar. 1996

NIFS-407 K. Kitachi, T. Oike, S. Ohdachi, K. Toi, R. Akiyama, A. Ejiri, Y. Hamada, H.Kuramoto, K. Narihara, T. Seki and JIPP T-IIU Group,
Measurement of Magnetic Field Fluctuations within Last Closed Flux Surface with Movable Magnetic Probe Array in the JIPP T-IIU Tokamak; Mar. 1996

NIFS-408 K. Hirose, S. Saito and Yoshi.H. Ichikawa
Structure of Period-2 Step-1 Accelerator Island in Area Preserving Maps;

Mar. 1996

NIFS-409 G.Y.Yu, M. Okamoto, H. Sanuki, T. Amano,
Effect of Plasma Inertia on Vertical Displacement Instability in Tokamaks; Mar. 1996

NIFS-410 T. Yamagishi,
Solution of Initial Value Problem of Gyro-Kinetic Equation; Mar. 1996

NIFS-411 K. Ida and N. Nakajima,
Comparison of Parallel Viscosity with Neoclassical Theory; Apr. 1996

NIFS-412 T. Ohkawa and H. Ohkawa,
Cuspher, A Combined Confinement System; Apr. 1996

NIFS-413 Y. Nomura, Y.H. Ichikawa and A.T. Filippov,
Stochasticity in the Josephson Map; Apr. 1996

NIFS-414 J. Uramoto,
Production Mechanism of Negative Pionlike Particles in H_2 Gas Discharge Plasma; Apr. 1996

NIFS-415 A. Fujisawa, H. Iguchi, S. Lee, T.P. Crowley, Y. Hamada, S. Hidekuma, M. Kojima,
Active Trajectory Control for a Heavy Ion Beam Probe on the Compact Helical System; May 1996

NIFS-416 M. Iwase, K. Ohkubo, S. Kubo and H. Idei
Band Rejection Filter for Measurement of Electron Cyclotron Emission during Electron Cyclotron Heating; May 1996

NIFS-417 T. Yabe, H. Daido,T. Aoki, E. Matsunaga and K. Arisawa,
Anomalous Crater Formation in Pulsed-Laser-Illuminated Aluminum Slab and Debris Distribution; May 1996

NIFS-418 J. Uramoto,
Extraction of K^- Mesonlike Particles from a D_2 Gas Discharge Plasma in Magnetic Field; May 1996

NIFS-419 J. Xu, K. Toi, H. Kuramoto, A. Nishizawa, J. Fujita, A. Ejiri, K. Narihara, T. Seki, H. Sakakita, K. Kawahata, K. Ida, K. Adachi, R. Akiyama, Y. Hamada, S. Hirokura, Y. Kawasumi, M. Kojima, I. Nomura, S. Ohdachi, K.N. Sato
Measurement of Internal Magnetic Field with Motional Stark Polarimetry in Current Ramp-Up Experiments of JIPP T-IIU; June 1996

NIFS-420 Y.N. Nejoh,
Arbitrary Amplitude Ion-acoustic Waves in a Relativistic Electron-beam Plasma System; July 1996

NIFS-421 K. Kondo, K. Ida, C. Christou, V.Yu.Sergeev, K.V.Khlopenkov, S.Sudo, F. Sano, H. Zushi, T. Mizuuchi, S. Besshou, H. Okada, K. Nagasaki, K. Sakamoto, Y. Kurimoto, H. Funaba, T. Hamada, T. Kinoshita, S. Kado, Y. Kanda, T. Okamoto, M. Wakatani and T. Obiki,
Behavior of Pellet Injected Li Ions into Heliotron E Plasmas; July 1996

NIFS-422 Y. Kondoh, M. Yamaguchi and K. Yokozuka,
Simulations of Toroidal Current Drive without External Magnetic Helicity Injection; July 1996

NIFS-423 Joong-San Koog,
Development of an Imaging VUV Monochromator in Normal Incidence Region; July 1996

NIFS-424 K. Orito,
A New Technique Based on the Transformation of Variables for Nonlinear Drift and Rossby Vortices; July 1996

NIFS-425 A. Fujisawa, H. Iguchi, S. Lee, T.P. Crowley, Y. Hamada, H. Sanuki, K. Itoh, S. Kubo, H. Idei, T. Minami, K. Tanaka, K. Ida, S. Nishimura, S. Hidekuma, M. Kojima, C. Takahashi, S. Okamura and K. Matsuoka,
Direct Observation of Potential Profiles with a 200keV Heavy Ion Beam Probe and Evaluation of Loss Cone Structure in Toroidal Helical Plasmas on the Compact Helical System; July 1996

NIFS-426 H. Kitauchi, K. Araki and S. Kida,
Flow Structure of Thermal Convection in a Rotating Spherical Shell; July 1996

NIFS-427 S. Kida and S. Goto,
Lagrangian Direct-interaction Approximation for Homogeneous Isotropic Turbulence; July 1996

NIFS-428 V.Yu. Sergeev, K.V. Khlopenkov, B.V. Kuteev, S. Sudo, K. Kondo, F. Sano, H. Zushi, H. Okada, S. Besshou, T. Mizuuchi, K. Nagasaki, Y. Kurimoto and T. Obiki,
Recent Experiments on Li Pellet Injection into Heliotron E; Aug. 1996

NIFS-429 N. Noda, V. Philipps and R. Neu,
A Review of Recent Experiments on W and High Z Materials as Plasma-Facing Components in Magnetic Fusion Devices; Aug. 1996

NIFS-430 R.L. Tobler, A. Nishimura and J. Yamamoto,
Design-Relevant Mechanical Properties of 316-Type Stainless Steels for Superconducting Magnets; Aug. 1996